DESIGN AND DEVELOPMENT OF A MICROMACHINED NON-INVASIVE PRESSURE-FLOW SENSOR SYSTEM FOR THE DETECTION OF PROSTATE CANCER IN MEN

by
Vikas Gupta

A THESIS SUBMITTED IN PARTIAL FULFILLMENT OF
THE REQUIREMENTS FOR THE DEGREE OF
MASTER OF APPLIED SCIENCE

in the School
of
Engineering Science

SIMON FRASER UNIVERSITY
February 25, 1997

Approval

Name: Vikas Gupta

Degree: Master of Applied Science

Title of Thesis: Design and Development of a Micromachined Non-Invasive Pressure-flow Sensor System for the Detection of Prostate Cancer in Men.

Examining Committee: Dr. P. Ho, Chairperson

Dr. M. Parameswaran
Senior Supervisor

Dr. Marek Syrzycki,
Supervisor

Dr. Shahram Payandeh
Examiner

Date Approved: FEBRUARY 25, 1997

Abstract

One of the most challenging concerns of Urosurgeons is to be able to diagnose a prostate cancer non-invasively. Existing techniques for diagnosis of prostate cancer are invasive in nature and lack concern for patient safety and comfort. These concerns have been the compelling force for urosurgeons to investigate new non-invasive techniques for the detection of prostate cancer in men. Urodynamic literature states that measurement of bladder pressure and urinary flow rate can be used in the evaluation of patients suspected of having prostate cancer. For example, a high bladder pressure due to an obstruction in the bladder neck and a low urine flow rate may be evaluated as a presence of potential prostate cancer. In normal conditions, the bladder pressure just before voiding is in the range of 40 to 60 mm of Hg, and the voiding flow rate in the order of 15 ml/s. A presence of obstruction in the bladder neck can result in the bladder pressure being as high as 80 mm of Hg or more and the flow rate lower than 10 ml/s. This thesis presents the design, fabrication and the preliminary testing results of a silicon micromachined pressure and flow sensor which are integrated together on a single silicon substrate. This thesis also presents the packaging of the device which will make the detection of prostate cancer possible non-invasively.

The pressure sensing principle is based on the change in the resistance of piezo-resistors due to stress (pressure). The well known simple anemometry technique being the flow sensing principle. The fabricated device has a pressure sensitivity of 1 mV/10 mm of Hg and a flow sensitivity of 0.98 mV/(ml/s). The working device exhibits the pressure range of 0 to 78 cm of Hg, and a flow range of 0 to 45 ml/s., and the time response of 100 msec., which are ideally suitable for the evaluation of prostate cancer.

dedicated to my parents, brothers and their families.

Acknowledgments

This thesis can not have come about without the help and encouragement from some very special people. I offer my sincere thanks to the following:

* My supervisor, Ash, for showing confidence in my ability and working with me and assisting me all throughout towards the progress of this project.
* Dr. Jim McEwen and Dr. Larry Goldenberg, from Vancouver General Hospital, for holding numerous technical meetings to explain anything and everything I needed (and not what I didn't need to) to know about the human (and not an elephant's) prostate.
* Dr. Ash for, also, carefully reviewing the thesis and for his valuable suggestions to make it more interesting thesis to read.
* Dr. Mak Paranjape for accompanying me to the interesting meetings with uroser geons to improve his technical knowledge regarding the human prostate and also, with the help of Ash, giving me atleast a million nicknames most of which are too embarrassing even to mention here.
* Dr. Marek Syrzycki and Dr. Shahram Payandeh for being the committee members and Dr. Paul Ho for chairing my thesis defense session.
* Micromachining colleagues - Jianming Chen, Manish Mehta, Shaoqing Wo, Dr. M. Paranjape for their constant help inside and outside the cleanroom.
* Dr. Eva Czyzewska, Bill Woods - for their help in various stages during the fabrica tion of the device in the cleanroom and also for helping me clean the mercury spill in the clean room (what a disaster it was!!).
* Bahram Ghodsian - the Guru of Frame Maker - for his valuable help with it.
* Anjali Atal for proof-reading my thesis and working on my language and grammar.
* Brigitte Rabold - for helping me with all the Graduate Studies Program related work.
* Family and friends - They all helped me to keep my sanity and constantly reminded me that there are pleasures other than a cleanroom that life has to offer.

Table of Contents

LIST OF TABLES

LIST OF FIGURES

Chapter1: Introduction

Silicon micromachining has become a fundamental tool for the fabrication of micromechanical devices and, in general, miniature sensors and actuators, also, commonly known as Micro-Electro-Mechanical Systems (MEMS). MEMS - tiny devices about the width of a human hair - are an offshoot of the technology developed to fabricate integrated circuits an silicon chips. While integrated circuits are designed to exploit the electrical properties of silicon, MEMS take advantage of silicon's electrical and mechanical properties. In the last decade a large number of micromachined sensors have been developed demonstrating new concepts and interesting physical principles have been applied to achieve better performing devices [1].

Researchers worldwide are continuing to pioneer more MEMS applications. As existing fabrication processes mature, new ones are developed, and the cost of MEMS device will become even lower, making it practical for a broader range of applications. While sensors are the most common types of MEMS, some of the most exciting work is aimed at making more MEMS mechanical devices and actuators. For example, generators, motors, and valves.

A cutting-edge application now under development is a silicon microphone that would provide voice recognition in games and other products [1]. Electrostatically actuated microrelays are being developed to facilitate two-way communication between homes and service providers, such as telephone and cable-TV companies. Some of the most recent innovative applications include sensors for automotive industries and medicine.

A large application of MEMS has come along with the use of the micromachined accelerometer in the widespread installation of airbags in new cars. Traditional accelerometers, which rely on piezoresistive technology, are one of the most widespread uses of

MEMS. Some new developments in the design of accelerometers will allow them to be used in the complex navigation and guidance system in airplanes and missiles. A new type of MEMS sensor - the rate gyro - has the potential to allow antilock-breaking systems to account for rotation.

Although MEMS sensors have found the greatest use in the automotive industry, the medical industry has sparked the development of some of the most innovative types recently. Medical science has always utilized the assistance of modern technology in many areas of clinical analysis and diagnostics. Physical and chemical measurement system aided with computerized controls are the most favored systems in clinics and hospitals. Recent advances and developments in the area of silicon micromachining has led to the fabrication of miniature sensors and actuators and this is finding innovative applications in novel diagnostic systems for medicine. The ability to integrate different types of sensors along with processing electronics on the same silicon substrate is now leading the way for the development of next generation diagnostic systems in medicine. For example, a whole new family of MEMS sensors detect the presence or absence of various chemicals [1]. Rather than measuring just one parameter, such as pressure or acceleration, some of the latest devices, known as microinstruments, are able to measure several values and process them to yield a more comprehensive answer.

Many of the first applications of microinstrumentation have been in the field of medicine. For example, devices soon to be commercialized include those that perform cytometry, detect heavy metals in blood samples, analyze other blood conditions, and perform polymerase chain reactions that replicate DNA for analysis. Along the development of microinstruments, a recent version of mass spectrometer - size of a hand-held calculator - contains the sample inlet, localization chamber, accelerating electrodes, drift chamber and detector array, all, intregrated on one single chip.

Along these lines we have investigated the design and development of an inte-

grated pressure-flow sensor for non-invasive detection of prostate cancer. The device is a micromachined silicon system that houses a pressure and a flow sensor on a single silicon substrate, capable of yielding a comprehensive diagnostic result in potentially detecting prostate cancer non-invasively.

1.1 Thesis Overview

This thesis discusses the design, fabrication, analysis and testing of the micromachined pressure-flow sensor for the non-invasive detection of prostate cancer. Chapter two gives a brief insight on the usage of various non-invasive tools in the medical field and also, in particular, for prostate cancer detection. A brief theory of non-invasive detection of prostate cancer is presented in the chapter three. Chapter four covers the design requirements of the sensors, their principle of operation, integration of pressure and flow sensors together and, also, the cross-talk between pressure and flow sensors. The device fabrication processes and device packaging are discussed in chapter five. In chapter six, the signal conditioning circuits are discussed. Experimental apparatus and testing procedures are presented in chapter seven. Testing results and discussion are provided in chapter eight, and finally, chapter nine summarizes conclusions reached in the thesis and a brief note on future work and other applications.

Chapter2: Non-Invasive Tools in medical field

This chapter discusses some of the non-invasive tools which are being implemented in the medical field nowadays.

2.1 Non-invasive Techniques

Large recovery time, infection risk, pain and trauma for the patient, hospital costs and postoperative complications are some of the few major problems associated with the invasive techniques commonly used in medical surgery[2]. Recent research and developments in the field of biomedicine are progressively giving surgeons as well as patients an option of going through surgery with much reduced risk and complications by introducing new techniques of non-invasive or minimal invasive surgeries. Such techniques are favored in preoperative visual inspection as well as in surgery.

Minimal Invasive Surgery (MIS) is the technique of operating on the internal organs of the body without damaging a much greater amount of surrounding healthy tissues. MIS techniques involve insertion of instruments and viewing equipment into the body through natural orifices or through punctures created by the surgeon. MIS is now being applied in an increasing number of routine operations. This rapidly growing field relies on video feedback and relatively primitive surgical instruments inserted through small incisions. Endoscopic surgery, one of the examples of the MIS, benefits the patient through the reduction of trauma, risk of inflammation, discomfort, postoperative complications, disruption of life-style and long-term disability. Advanced endoscopic surgical devices, to give doctors more dextrous control as well as tactile feedback and even automated suturing, are being developed [2].

Non-invasive techniques, on the other hand, involve no insertion of any instruments inside the human body in order to perform diagnostic or therapeutic functions. In particular, non-invasive tools are being used more and more in various small size hand-held self-use detection systems. Blood monitoring systems and early detection of cardiac disorders are only few of the examples. Research and development firms are developing a portable, non-invasive blood sugar meter, of the size of a pocket calculator which uses high frequency electromagnetic fields to measure the glucose levels through the finger, that people with diabetes can use themselves at home [1].

Researchers and surgeons in the Urology department, worldwide, have, recently, shown a growing interest in the use of non-invasive techniques for the detection of prostate cancer in men. This growing interest in non-invasive techniques is also due to the fact that existing detection techniques are invasive in nature and often not favored by either urosurgeons or patients.

2.2 Invasive Techniques to detect Prostate Cancer

This section explains some of the most common existing techniques used in the detection of presence of prostate cancer (from ref. [3]).

2.2.1 Ultrasonography

The technique of imaging an object using the ultrasound beam based on the doppler method is called the ultrasonography. A number of approaches to sonographic imaging of the prostate have been utilized. The most common approaches today are the transabdominal, transperineal, transurethral, and the transrectal, or more appropriately the endorectal, technique in which the sonographic probe is placed within the rectum.

The transabdominal approach was the first method used to scan the prostate. A variety of conventional abdominal scanners and probes were utilized and some valuable information is obtainable with this approach, primarily a general assessment of prostate size and an evaluation of bladder emptying by measuring the postvoid residual. Imaging system in this technique does not provide a clear image of zonal anatomy of prostate, thus making the detection of the enlargement of the prostate less accurate.

In the transperineal approach, the placement of imaging probe with the prostate was improved, however, the technique has fallen into disfavor because of the relative inferiority of the images obtained owing due to beam scatter from perineal fat and other surrounding muscles.

Transurethral prostatic ultrasonography has had waxing and waning popularity. The prostate can be imaged with a sonographic probe placed through a cystoscope. The potential advantage to transurethral ultrasonography is that with the probe placed within the urethra, a more detailed image of the prostate can be optimally obtained. The lack of its ability to provide the peripheral zone image of the prostate, along with the necessity for cystoscopy with a fairly large instrument, have made this technique less favorable too.

Transrectal ultrasonography, being the most commonly used technique among others, is the technique in which the imaging of the prostate is performed by placing the sonographic probe within the rectum. In transrectal ultrasonography, the probe is placed in such a way that it is possible to scan the peripheral as well as the axial anatomy of the prostate, thus providing valuable information such as asymmetry, inhomogeneity, and enlargement of the prostate. The following are some of the instruments used in transrectal ultrasonography.

Handy-Type transrectal Probe: The most basic model for the method, a round oscillating disc is attached at the tip of the rotative inner tube inside the fixed outer tube. This device provides a horizontal section of the prostate with radial scanning. Ultrasound

frequency used, for the method, is 5 to 7.5 MHz.

Chair-Type Equipment for Transrectal Ultrasonography: Chair type equipment was more efficient and allowed higher standards of reproducibility than handy-type probes. The equipment consists of a chair, in the seat of which a hole has been made to allow the passage of a special intracorporeal probe, set up beneath it.

Electronic Linear Array Transrectal Probe: Recent development of a linear array transducer makes it possible to reduce the size of transducer suitable for transrectal insertion.

2.2.2 Invasive Pressure-Flow Study

An obstruction in the bladder neck is considered to be a cause of voiding disorder in men. Voiding disorder can further be analyzed by studying the pressure-flow pattern of urine during the voiding. Existing technique, to perform the pressure-flow study, is invasive in nature where a sub-micron size tip transducer catheter is introduced into the urethra under x-ray monitoring. Intraurethral pressure is measured at various sites in the urethra during the voiding. The pressure and flow patterns are recorded and studied to diagnose the presence of an obstruction in the bladder neck.

2.3 Motivation

Although prostatic ultrasonography is a well established technique in the detection of prostate cancer, it is invasive in nature and requires concern for patient safety and comfort as well as the establishment of a positive physician-patient relationship.

In pressure-flow study also, the insertion of catheter into urethra causes a great deal of discomfort to the patient. This discomfort may sometimes affect the natural voiding pattern and thus, results in a wrong pressure-flow signature.

These problems sparked the research towards the development of a **non-invasive** technique for the diagnosis of detection of prostate cancer in men. A very simple idea of development of a sensor system was presented which would measure the pressure flow rate during the voiding non-invasively.

In the following chapter, a brief theory on the non-invasive detection of prostate cancer is presented.

Chapter3: Non-Invasive Detection of Prostate Cancer

3.1 Theory of Non-invasive detection of Prostate Cancer

One form of urinary dysfunction is caused by the cancer of prostate. Early signs of prostate cancer can be mistaken for a blockage of urinary tract by a kidney stone and it is essential to diagnose the condition quickly and correctly. While surgery is one potential option for the diagnosis, a non-invasive diagnosis is always preferred by the doctors as well as patients. Urodynamic literature states that measurement of bladder pressure and urinary flow can be used in the evaluation of patients suspected of having prostate cancer. For example, a high bladder back pressure due to an obstruction in the bladder neck and a low urine flow rate may be evaluated as a presence of potential prostate cancer. In normal conditions, the bladder pressure just before voiding is in the range of 40 to 60 mm of Hg, and the voiding flow rate in the order of 15 ml/s.The presence of an obstruction in the bladder neck can result in a bladder pressure as high as 80 mm of Hg or more and a flow rate lower than 10 ml/s.

Normal bladder voiding is caused by the contraction of bladder muscle called detrusor[5]. Normal bladder voiding requires mechanical energy, which is supplied by the detrusor through muscle contraction, namely a conversion of biochemical energy into mechanical, voiding work. The voiding work (W) is proportional to the volume (V) and the pressure (p)[5]

$$W = p \cdot V$$

This can be expressed in terms of power (P)[5]. Because the flow rate represents the change of bladder volume in time, the voiding power (P) is proportional to the flow rate (Q) and pressure (p):

$$P = \frac{W}{t} = p \cdot Q$$

Hence, for a given power, a high pressure can occur only in combination with a low flow rate and, conversely, a high flow rate is possible only with a low pressure. This inverse relation is a general feature of biological power sources. For example, our skeletal musculature either can contract fast at minimal load or can move a heavy load slowly.

When we consider the discharge of the urine outside the body, the diameter of the urethra (urinary tract) should be taken into account. Urodynamic research during the past 20 years has established a realistic fluid dynamic approach by an analogy with the flow conditions in collapsible and distensible soft conduit that more closely represents urethral structure and function [19]. Fluid will flow from a higher to a lower pressure in a conduit with a velocity (v) proportional to the pressure difference, which for the bladder outlet is approximated by the detrusor pressure (p_{det}). The volume moving through a cross section (A) during a period of time (i.e., the flow rate) will depend on the size of the conduit and on the flow velocity. Therefore, the relation between pressure and flow rate can reasonably be described by a simple formula[5]:

$$Q \sim A \cdot \sqrt{(p_d) - (p_m)}$$

which basically says that the flow rate increases in proportional to cross section and the square root of the pressure. It is a reasonable simplification to ignore the minute fluid energy losses in this approximation. Here, A is the cross-sectional area of the urethra, p_d is

the pressure applied by the detrusor and p_m is the minimum pressure required to open the urethra for discharging the urine. Figure3.1 illustrates the pressure - flow rate response for a typical urinary discharge.

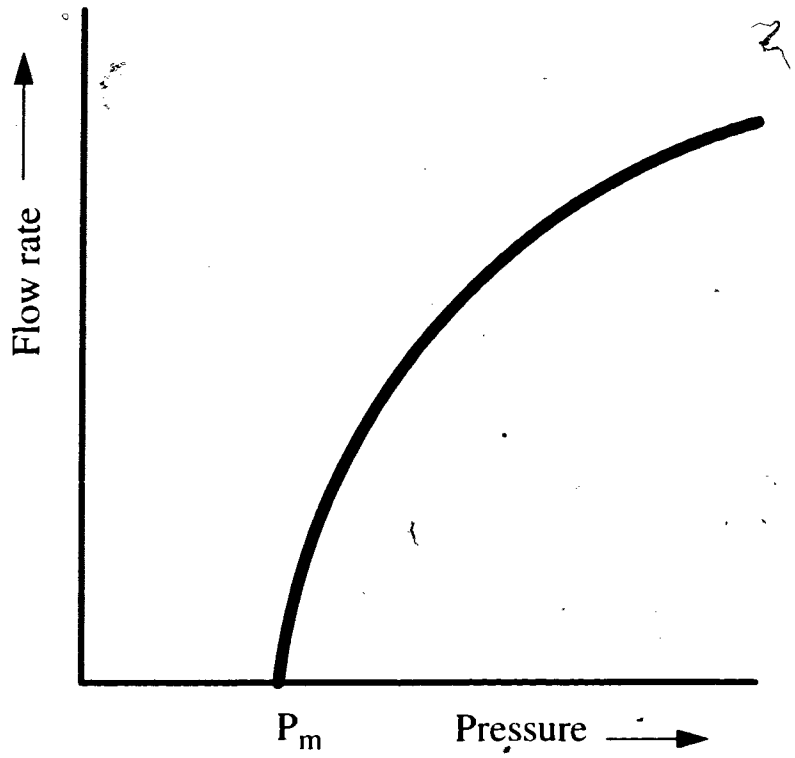

Figure 3.1: The urethral pressure-flow response[5]

In order to perform an evaluation study to diagnose a potential prostate cancer, the practical way is to measure the bladder pressure and the urine voiding flow rate simultaneously with respect to time. Urodynamic literature reports that three characteristic signature pressure-flow patterns can be observed for three distinct conditions[5]. Figure 3.2a shows the pressure and flow rate with respect to time for normal condition. If there is a constrictive obstruction, say caused by a kidney stone, it will result in the pressure-flow signature as shown in figure 3.2b. A peak in the bladder pressure will be observed while the flow rate remains lower than normal and is steady with respect to time. Figure 3.2c demonstrates the

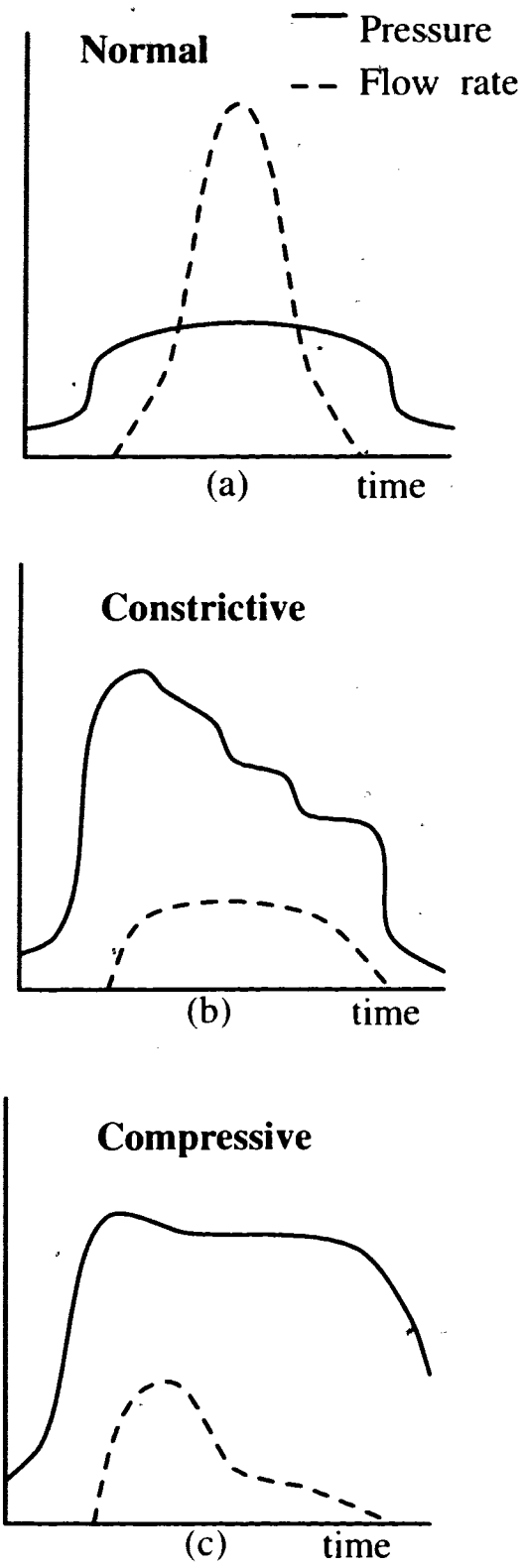

Figure 3.2: Characteristics pressure-flow signatures for various obstructions

condition for compressive obstruction, for example caused by the enlargement of the prostate. This characteristic signature is marked by a peak in the flow rate while the pressure remains reasonably steady with respect to time. Since these pressure-flow characteristics can be determined by properly measuring the voiding function of a patient, diagnosis of prostate cancer can be done non-invasively by a sensor that combines the pressure and flow sensing in a single package. It should be noted that for the device to function correctly, both the measurements should be independent (measuring pressure should not effect the measurement of flow and vice-versa). With the advent of micromachining technology, pressure and flow sensors can be implemented on a single substrate for this type of diagnostic purpose and this has been the main objective of this thesis. The following chapter discusses the design of the sensors [5].

Chapter4: Sensor Design

In the past decade, a significant amount of research has been performed in the field of design and development of pressure and flow sensors, for different purposes. Although there are numerous kinds of pressure sensors and flow sensors, based on different operating principles available in the market and the literature, for the sake of our interest we will limit our discussion to only small size sensors (microsensors) which could potentially be useful in this application. This section discusses, very briefly, the design and working principles of few pressure and flow sensors which are of relevance to our application.

4.1 Pressure Sensors

4.1.1 Resonant Pressure Sensor

Typically, in such sensors, a micromachined resonant structure is attached to the diaphragm whose frequency shifts with pressure. One such example is a torsional resonant pressure sensor. The deflection in the diaphragm modifies the torsional spring-constant and thus the resonant frequency of the coupled oscillators.

Though the advantage of the resonant structure over the static structure is the improved accuracy and lower hysteresis, it suffers from its non-linear response and high sensitivity to temperature [13].

4.1.2 Capacitive Effect

In a typical capacitance transducer, one plate is fixed while the other is free to move in response to an external force or pressure. The movement of the free plate changes the capacitor spacing and therefore results in a change in the capacitance. The dependence of capacitance on plate area, plate separation, and permittivity of the medium between the plates of the capacitor are used as a means of converting a displacement (pressure) to a detectable electrical output.

Capacitive pressure sensors yield excellent accuracy and sensitivity. The main drawback associated with the sensors are the fact that they produce relatively small change in capacitance with pressure. A serious problem with capacitive sensors is that the leads connecting the pressure sensor to the outside tend to show stray capacitances which are of the same order as the sensor capacitance. Such type of sensors are, also, highly sensitive but are generally difficult and expensive to fabricate. Also, special circuit techniques are necessary to be able to register these small changes accurately and to avoid stray capacitive effects which may introduce error or uncertainty in the pressure measurement [16].

4.2 Flow Sensors

4.2.1 Capacitive Effect

There has been recent interest in the use of capacitive flow sensor in which the gas flow rate generates the pressure differential across the fluidic channel, which in turn, is measured by a capacitive pressure sensor. A resolution of 1 fF has been reported which corresponds to a change in pressure of 0.13 Pa.

Temperature sensitivity and leakage currents are the main drawback associated with this design of flow sensor [13].

4.2.2 Resonant Bridge Flow Microsensor

A resonant bridge flow microsensor is based on the frequency shift of a resonating microbridge. Thin phosphorous doped polysilicon resistors are embedded within the bridge for the thermal excitation and piezoresistive sensing of vibrations.

Potential advantages of resonant microstructures are their high sensitivity, fast response and good stability. The main drawback of the sensor are large power consumption and is not suitable for operation in the fluid medium.

Most of the sensors discussed above have drawback which make these designs unsuitable to use in the fluid medium. In the following section, a design for pressure and flow sensor is proposed which can be implemented to use in the fluidic medium [13].

4.3 Possible Solution

To be able to measure the bladder pressure and urinary flow rate, it is evident that pressure and flow sensors must be able to operate in the fluidic medium. It should also be noted that the sensors should be designed and assembled such that they could measure the bladder pressure and urinary flow rate non-invasively. The non-invasive measurement also suggests that the sensor should be miniature in size so that it could fit in the wall of a plastic tube which would have about same circular cross-sectional area as of the urethral tube, roughly the range of 2 - 6 mm. Due to these critical restrictions, the sensors based on the bulk micromachining technology are the natural candidates for this application.

Silicon Micromachining is the application of silicon planar IC processing techniques to the selective etching of silicon and other films in order to fabricate microstructures. Micromachining technology not only requires all the conventional IC processing techniques but additional ones for new passive materials or active materials. With this combination of technologies it is possible to accurately and economically fabricate carefully designed microsensors on a batch fabrication approach.

This thesis presents the design and fabrication of a pressure and flow sensor which are integrated together on the single silicon substrate and is packaged in such a way that it makes the non-invasive measurement of pressure and flow rate possible. This thesis also presents the results of the preliminary testing of the device. The sensors are fabricated using bulk micromachining technology.

4.4 Design of the sensor

This chapter describes the design and fabrication of the pressure-flow sensor system for the early detection of prostate cancer.

4.4.1 Design requirements

The following objectives/requirements were put in perspective before designing a suitable pressure-flow sensor for the detection of prostate cancer:

1) The sensor must be designed to work non-invasively, i.e., no part of the device to be inserted into the body.
2) The sensor must be able to operate in a liquid medium.
3) The sensor should be miniature in size.

4) The pressure and flow sensors should preferably be integrated together and should be able to operate independently providing simultaneous reading.
5) The sensor should atleast operate in the pressure range of 0 to 120 mm of Hg and flow rangeof 0 to 25 ml/sec.

Based on these, a simple design of pressure and flow sensor was proposed.

In this design, pressure sensing is based on the piezoresistive effect and flow sensor being based on heat transfer principle. The integration of these two sensors together in a single silicon substrate makes it a unique design. Fig 4.1 illustrates the proposed design of pressure-flow sensor.

4.5 Sensor Operating Principle

4.5.1 Pressure Sensor

It can be noted from figure 4.1 that all the resistors are placed on the thin portion of the silicon (membrane) created by the micromachining process. Figure 4.2 shows the top view of the pressure sensor. Resistors P_1, P_2, P_3 and P_4 are used for sensing the pressure. If the membrane experiences deformation due to pressure difference, this will introduce stress on the membrane as well as the resistors P_1, P_2, P_3 and P_4. These resistors are piezoresistors and the operation of the pressure sensor is based on piezoresistive effect.

In the piezoresistive effect, the relative change in resistance or resistivity is proportional to the mechanical stress vector σ_m [15]. This can be expressed as:

%!

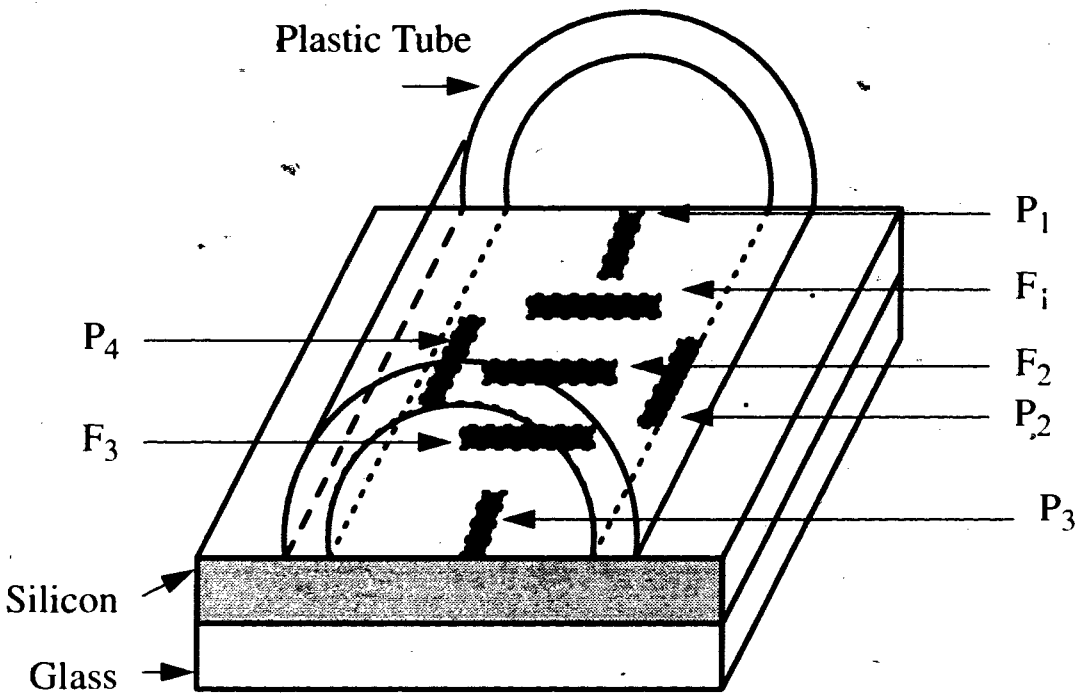

Figure 4.1: Proposed Pressure-Flow Sensor
(P_1 - P_4 --> Pressure Sensing Resistors
F_1 - F_3 --> Flow Sensing Resistors)

$$\frac{(\Delta R_i)}{R_i} = [\Pi_{ij}] \cdot \sigma_{mj}$$

where $[\Pi_{ij}]$ is the *ij*th piezoresistive coefficient of the material matrix.

In silicon, there are only three non-zero piezoresistive coefficients, namely Π_{11}, Π_{12} and Π_{44} due to the centrosymmetric structure. Piezoresistors can be readily fabricated

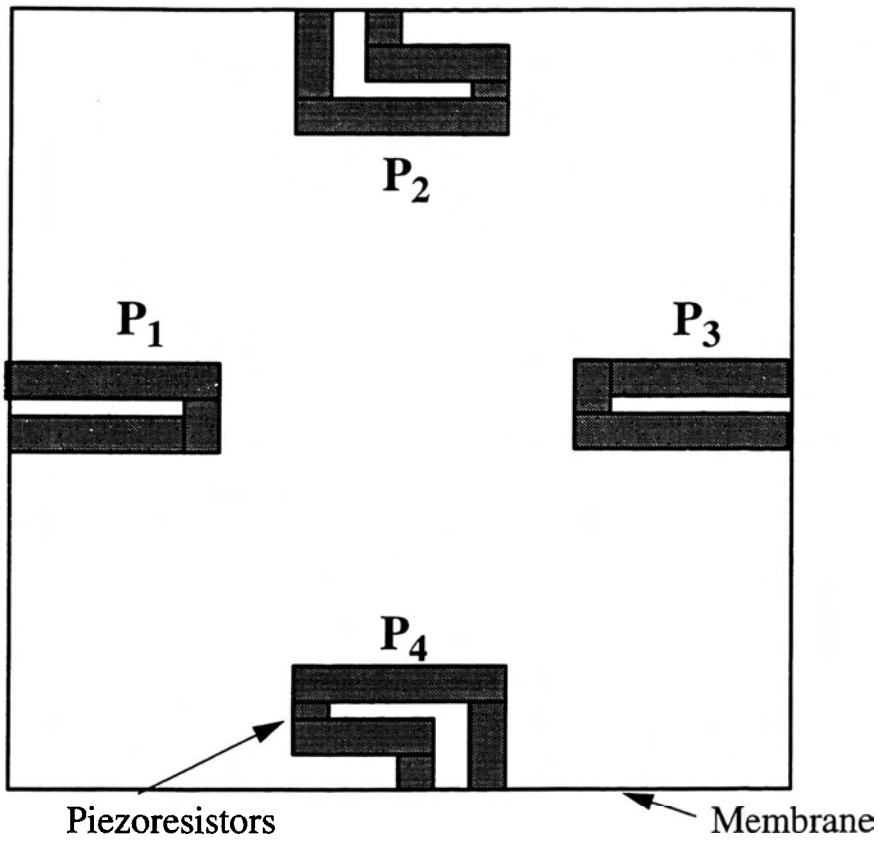

Figure 4.2: Top view of the pressure sensor design

by diffusing p-type materials into the bulk silicon crystal [15].

The fractional change in resistance of a piezoresistor is related to the parallel and transverse piezoresistive coefficients, Π_p and Π_t, and stress σ_p and σ_t [15]:

$$\frac{(\Delta R)}{R} = \Pi_p \cdot \sigma_p + \Pi_t \cdot \sigma_t$$

The exact fractional change in resistance depends upon the crystal orientation used, e.g. (100), (110) or (111) crystal planes.

It is, sometimes, more convenient to express the effect in terms of strain ε_m rather than stress. The gauge factor, K, is a measure of the strain sensitivity of a material. The resistance change can be found from the sum of the longitudinal and perpendicular gauge factors and strains,

$$\frac{(\Delta R)}{R} = K_p \cdot \varepsilon_p + K_t \cdot \varepsilon_t$$

A simple design consists of a thin silicon diaphragm with piezoresistors diffused into the surface that measures its deflection. Single crystal silicon is an excellent material for pressure sensors because practically no creep or hysteresis occurs. Diffusing two p-type resistors into an n-type silicon diaphragm of surface orientation (100) and another two in perpendicular direction to the first two results in the following equation[15]:

$$\frac{(\Delta R)}{R} = \frac{\Pi_{44}}{2}(\sigma_p - \sigma_t)$$

where, Π_{44} being the coefficient which is more important than the other coefficients for p-type resistors.

Since boron-diffused silicon is piezoresistive, measurement of these resistors in the Wheatstone bridge configuration can be used for determining the pressure. The placement of pressure sensitive resistors on the membrane is done such that it experiences maximum resistance change when the membrane deforms due to pressure difference.

4.5.2 Flow Sensor

In order to configure the flow sensor, as shown in figure 4.3, the resistor F_2 is used as the heater element and resistors F_1 and F_3 are used as temperature sensors. When there is no fluid flow, the heat produced by the heater F_2 will be equally distributed to F_1 and F_3. When there is a fluid flow, this heat distribution will be modified which will result in an imbalance in the heat distribution and that can be detected by measuring the resistance of F_1 and F_3 in a differential fashion. The heat flows according to the equation:

$$\Delta T = C (T_s - T_f) v$$

where T_s is the temperature of the sensor, T_f the temperature of the fluid,

ΔT is the temperature rise between T_1 and T_2,

C is the specific heat of the fluid,

v is the flow rate

The output voltage of each temperature sensor (V_{T1} and V_{T2}) is proportional to the temperature at each measurement point, F_1 and F_3 (T_1 and T_2). The heat rise ($\Delta T = T_2 - T_1$) is linearly related to the flow rate. The precise equation relating the flow rate and the temperature difference is more complicated in practice because it is determined by the heat transfer coefficients across the boundary layer.

The flow sensor elements are located on top of the free standing silicon membrane, as opposed to silicon bulk, in order to thermally isolate the heating element from the substrate so that most power passes into the fluid medium, and as little as possible is lost in the substrate. To minimize the heat loss during the flow measurement, a very thin membrane is formed.

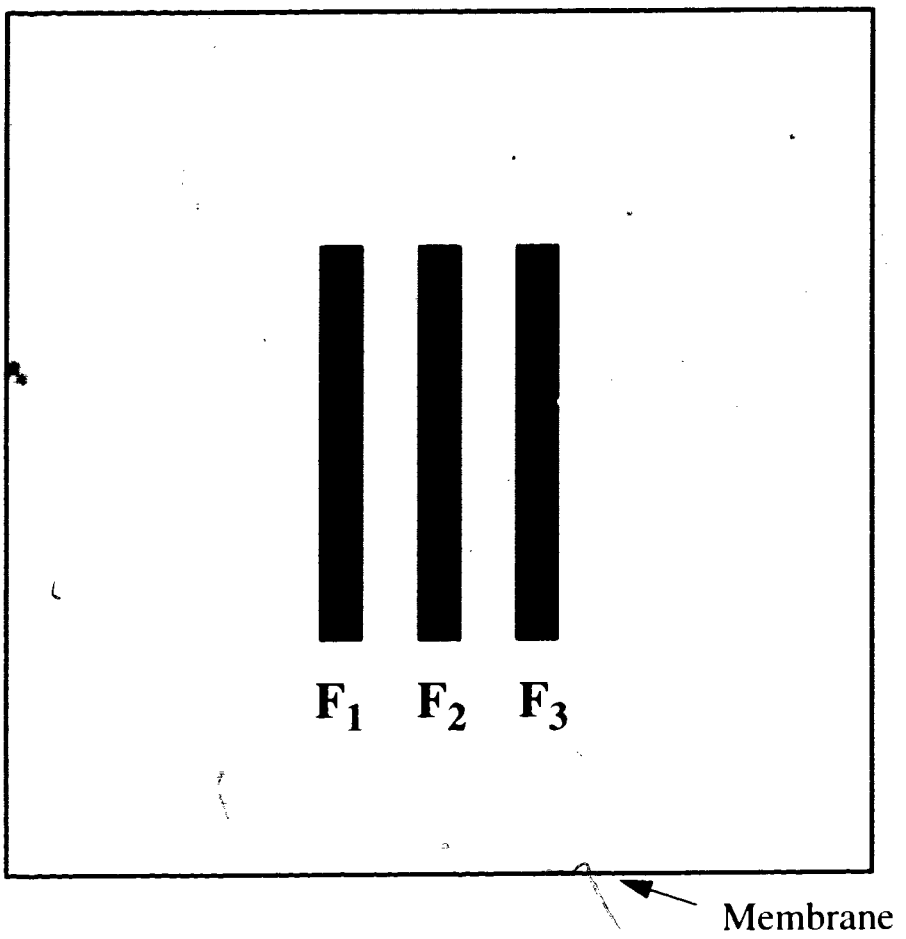

Figure 4.3: Top view of the flow sensor design

4.6 Integration of pressure and flow sensor

This thesis presents the integration of pressure and flow sensor together on one single silicon substrate. Since, simultaneous recording of pressure as well as flow patterns during voiding, with respect to time, is required in this application, there is a need to somehow integrate these two sensors together on one single chip. The idea of integrating

two sensors also, considerably, reduces the overall size of the sensor.

As explained in the previous section, both, pressure and flow sensors have their sensing elements made out of boron diffusion into the silicon substrate. Also, since, both, pressure and flow sensing elements are located on a thin silicon membrane, required for elasticity (pressure sensor) and thermal isolation (flow sensor), it makes these two sensors ideally suitable to integrate them together and to be able to fabricate them using a common fabrication process.

Due to the simplicity of their design, two sensors are combined together such that the flow sensing elements are situated on the middle of the membrane and the pressure sensing elements more or less on the periphery of the membrane. The integration of two sensors together is illustrated in figure 4.4.

Since both pressure and flow sensors, are located on the same silicon chip, it is important to make sure that flow and pressure sensors don't interfere with each other in their operation. A simple signal conditioning electronic circuit was used to output the pressure and flow signals without interference between each other.

4.7 Cross-Talk

It should be noted that both the pressure and flow sensors operate on the basis of change in resistance. Since both sensors are located on the same micromachined membrane, flow sensing resistors can change its resistive value when the pressure is applied to the membrane. Similarly, the pressure sensing resistors will change its resistive value when the flow sensor is initiated. This effect can be considered as Cross-Talk and this can be classified into two main categories.

1) Influence of pressure on flow measurement, and

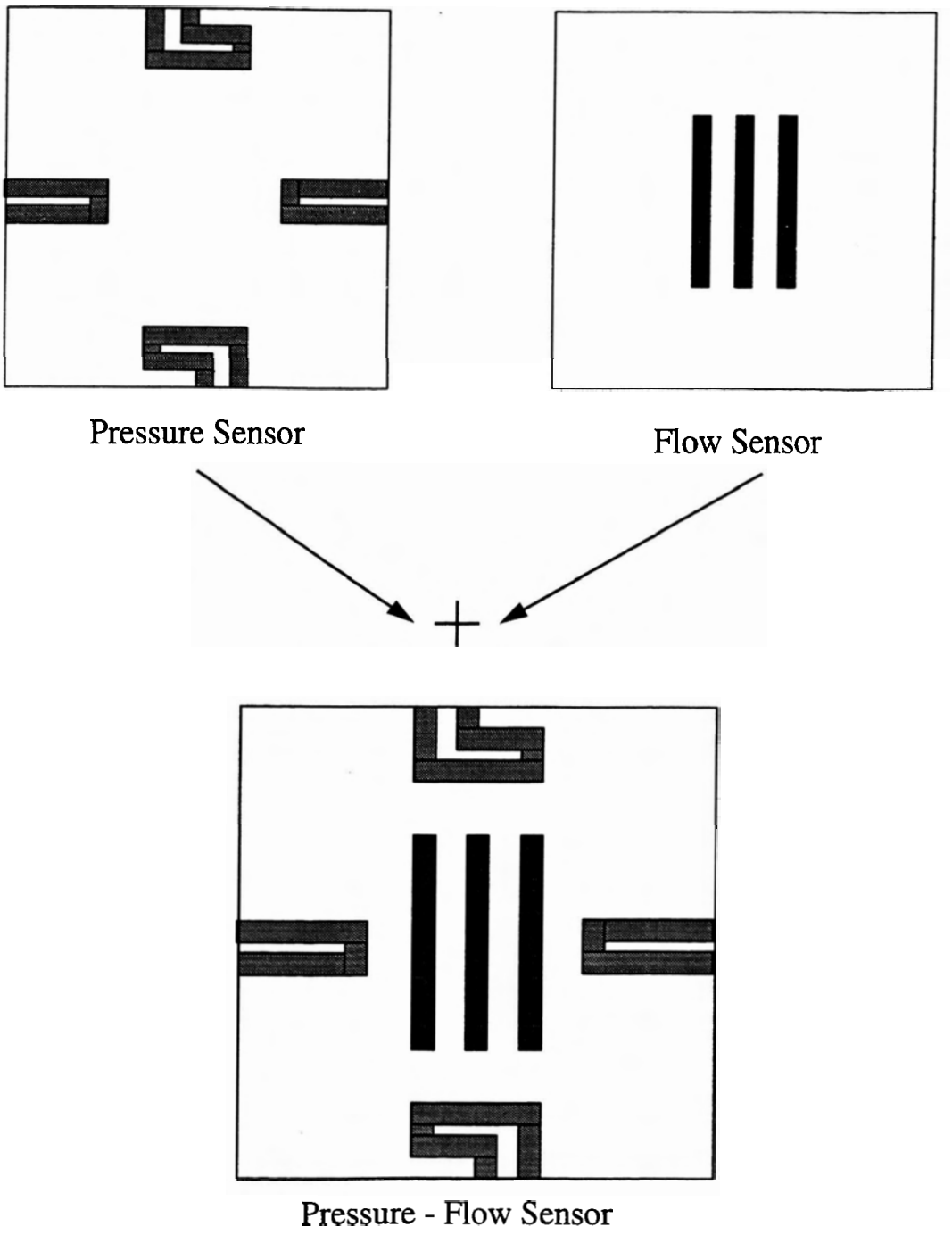

Figure 4.4: Integration of Pressure and Flow Sensors in one substrate

2) Influence of flow on pressure measurement.

4.7.1 Influence of Pressure on flow measurement

Deflection of the membrane, due to pressure, causes the pressure-sensitive stress in the flow sensing elements particularly in the temperature sensing elements F_1 and F_3 (see figure 4.3). This stress will result in an increase in the resistance of F_1 and F_3 which may be considered as an interference component in the flow measurement. The amount of change in resistance depends on the magnitude and the direction on the stress produced in the element. Since, at any given pressure, the direction of the stress produced in the membrane is away from the centre of the membrane and towards the edges of the membrane, the stress produced in F_1 and F_3 will be in the directions as illustrated in figure 4.5 [10].

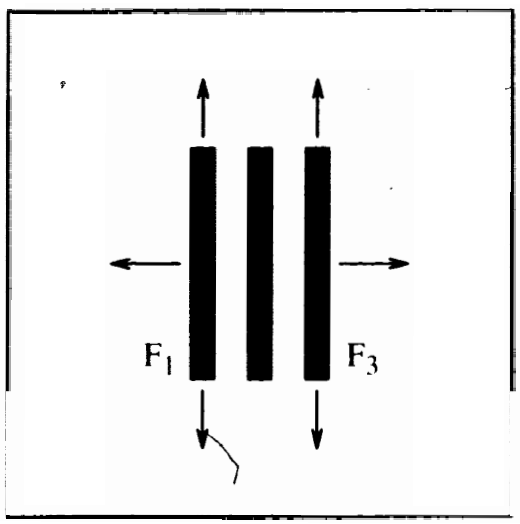

Figure 4.5: Illustration of direction of stress on flow sensor due to pressure

Due to the symmetry in the structure of the flow sensing elements, the stress pro-

duced in F_1 and F_3 will be fairly equal in magnitude and thus causes an equal amount of change in resistance in both F_1 and F_3. Since, the flow sensing method is based on the differential measurement between F_1 and F_3, the effect of pressure on the flow sensing can be brought down to a very small value. Further, the electronic circuit employed for signal conditioning can be incorporated to nullify any imbalance caused due to potential mask errors / processing errors in fabrication.

4.7.2 Influence of Flow on pressure measurement

The effect of flow sensor on pressure measurement is temperature based. The flow sensor, which operates on the thermal effect, has a heater element which is heated by applying a constant electrical voltage across it. The dissipation of heat through the silicon material into the pressure sensitive elements causes a rise in temperature of the piezoresistors. Since, the piezoresistors are temperature-sensitive, the rise in temperature is picked up by the piezoresistors as a temperature-induced interference in the output. The effect of heat transfer on pressure sensor due to flow sensor is illustrated in figure 4.6.

4.8 Elimination of Cross-Talk

The cross-talk, discussed in the previous section, can easily be reduced considerably, if not eliminated completely, by using an appropriate electrical signal conditioning circuit.

Pressure measurement in Wheatstone bridge configuration is one easy way of eliminating the interference in pressure measurement. Implementation of a differential

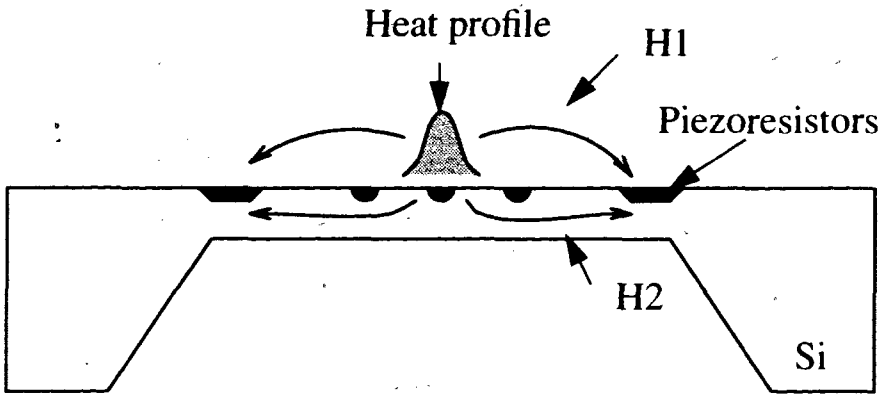

Figure 4.6: Illustration of cause of heat transfer on pressure sensor

H1 --> Heat conduction by the surrounding medium
H2 --> Heat conduction through the Si.

amplifier, using op-amps as a signal conditioning circuit for the flow sensor provides flow outputs without the interference from pressure sensor. Both these circuits and their operations are discussed in detail in chapter six.

Chapter5: Fabrication and Packaging of the Sensor

5.1 Fabrication of the device

The fabrication of the integrated pressure-flow sensor is accomplished in two steps; namely, the fabrication of the silicon sensor part and the bonding of the silicon part with a glass plate using the anodic bonding technique. To fabricate the silicon sensor part, a special type of silicon wafer was used. This wafer has a very thin (~2 μ) silicon dioxide layer buried about 15 μ deep inside the silicon wafer. Since silicon dioxide acts as an insulator, this specialized wafer is called Semiconductor-On-Insulator (S-O-I) wafer. In our application, the silicon dioxide layer acts as an etch stop for EDP etching, thus, produces 15 μ thick membrane after anisotropic etching in EDP. The cross-section structure of the S-O-I wafer is shown in fig 5.1.

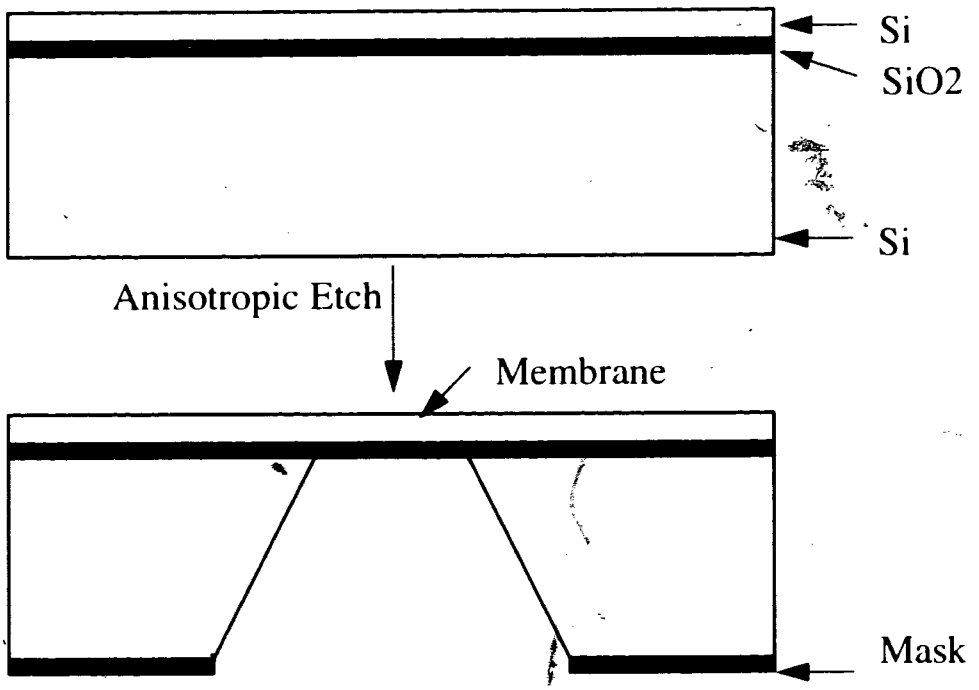

Figure 5.1: Anisotropic etching of the S-O-I wafer

In the following section, the fabrication processes of the silicon sensor part is described.

5.1.1 Fabrication of the Silicon Sensor Part

The sensor was fabricated using the following process flow:

1) Layout Design of the Sensor

2) Mask Making

3) Wafer Cleaning

4) Oxidation

5) Patterning (back side)

6) Silicon Dioxide Etching

7) Anisotropic Silicon Etching

8) Diffusion (front side)

9) Metallization

10) Aluminium Etching

11) Spin-On-Glass

5.1.1.1 Layout Design of the Sensor

In order to fabricate the sensor, the silicon wafer goes through various processing steps and some of the steps require lithography. The layout designs are drawn using a CAD package called KIC. The designs are drawn in the same dimension as that of the actual sensor.

In our design, the sensor layout was designed consisting of three different layers, one each for silicon etching, diffusion and metal etching process. Proper positioning of these different layers in the final layout is very critical and all precautions are taken in doing so. Special features such as alignment marks are added in the layout to be able to perform double-side photolithography. The layout design of the pressure-flow sensor is given in Appendix B.

5.1.1.2 Mask Making

The design file of the layout, in postscript format, is sent to a desktop publishing company which generates a negative image of the actual layout on a photographic film. The image on the photographic film is, in turn, transferred onto a photographic glass plate, called the mask plate. Transfer of pattern from the photographic film onto a mask plate is done in-house at Simon Fraser University. These glass mask plates with patterns on them are the ones which are actually used in the fabrication processes for patterning.

5.1.1.3 Wafer Cleaning

The first step in the fabrication process was cleaning the silicon wafer in preparation for oxidation. The wafers are cleaned with a cleaning process called standard RCA

clean. This removes contaminants from the surface allowing the formation of a homogeneous oxide layer in the subsequent step. The cleaning process consists of three steps. Table 5.1 lists the process for the cleaning procedure [2].

Table 5•1: RCA Clean Process Steps

Process Step	Process	Time & Temperature
1	Immerse in Solution 1: 5:2:1 mixture of DI water:H_2O_2:NH_4OH	10 minutes at 75-80 °C
2	DI Water rinse	3 mins.
3	Immerse in Solution 2: 10:1 mixture of DI water:HF	30 seconds at room temp.
4	DI Water rinse	3 mins.
5	Immerse in Solution 3: 5:2:1 mixture of DI water:H_2O_2:HCl	10 mins at 75-80 °C
6	DI water cascade rinse	3 rinses; 5 min each

5.1.1.4 Oxidation

A layer of silicon dioxide (SiO_2) was grown on the surface of the <100> single crystal silicon wafer. The oxide serves as the mask for the anisotropic etching of silicon subsequently. Oxidation is performed by placing the wafers into an 1100 °C furnace with oxygen and steam flow. The chemical reaction for this process can be simply stated as:

$$Si + O_2 \text{ --> } SiO_2$$

This process results in a uniform layer of silicon dioxide covering the entire surface of the silicon wafer.

The procedure for the oxidation process is as follows. The RCA cleaned wafers are loaded onto a quartz furnace boat. The furnace is preheated to a stable 1100 ^{o}C and a 1.9litre/s nitrogen gas flow is maintained. The boat is then slowly and carefully inserted into the furnace so that the increase in the temperature of the wafer is gradual in time. This step is very crucial because otherwise because of the sudden temperature shock the wafer may develop some internal defects. When the wafer is stable at 1100 ^{o}C, then dry oxygen is bubbled through a boiling deionized water into the furnace. Oxidation of wafer with oxygen and the water vapor is called wet oxidation. Wet oxidation yields faster and thicker oxide layer compared to the dry oxidation, which is performed in absence of water vapor. After the oxidation duration is over, then oxygen flow is then stopped and the nitrogen flow at same rate is resumed. The wafers are then carefully removed by pulling the wafer boat slowly out of the furnace.

The actual oxidation process was carried for 60 mins. According to the standard calibration curve for oxide thickness versus oxidation time, an oxidation time of 60 mins produces a thickness of 0.6 μ which is the desired thickness for masking purpose.

5.1.1.5 Lithography and Patterning

Lithography is the process of imprinting a geometric pattern from a mask onto a thin layer of material called a photoresist (a photo-sensitive material). Photolithography technique takes advantage of the following two main properties of a photoresist material:

1) exposure to UV radiation causes a change in the solubility of the photoresist.

2) the unexposed region of photoresist resists the attack by the developer and thus, the developer attacks only the exposed region of resist.

The wafer with oxide layer was then to be prepared for the silicon etching. To do so, the silicon wafer is coated with a thin layer (~1 μ) photoresist (Shipley SPR 2-1.0L). The spinner used in this process had a vacuum chuck operating at 4000 rpm for 30 sec. At this speed the photoresist material spreads evenly on the wafer. The wafer, coated with photoresist, is then kept in the furnace for soft baking at 90 ^{o}C for about 20 min.

After soft-bake, the wafer is ready for patterning. Quintel mask aligner was used to expose the wafer. Using etching mask, the wafer, on the resist side, was exposed (for 35 sec) to UV radiation through the mask plate. The exposed wafer was then developed in the AZ 351 developer for 45 sec and was finally rinsed carefully in the DI water. The wafer, after drying, was cured in a hard bake oven at 110 ^{o}C for 30 min [2].

At this point, we have a wafer with a pattern in the resist material on top of the SiO_2 layer. The next step is to etch the exposed underlying silicon dioxide regions.

5.1.1.6 Silicon Dioxide Etching

To etch the underlying oxide, the wafer is kept in the solution of buffered oxide etch (BOE). BOE is a 6 to 7 parts of NH_4F added to one part of HF. The chemical reaction for the process is:

$$SiO_2 + 4HF \rightarrow SiF_4 + 2H_2O$$

BOE is extremely stable and can be stored for considerable time without degradation. BOE is a reasonably selective etch for oxide and it does not etch silicon. However, HF attacks photoresist to some extent, although the addition of ammonium fluoride reduces this effect. In general, the oxide adhesion is adequate to withstand the etch time of about 30 mins.

To identify the completion of the etch, the wetting properties of the silicon and the

silicon dioxide is employed. In nature, oxide surface is hydrophilic and is easily wetted by water. On the other hand, silicon is hydrophobic and repels water. Therefore, a completely etched silicon substrate, dipped in water, will shed the water instantly when removed out of the water. Usually, a 0.5μ thick oxide layer takes about 6-7 mins to etch completely..

The wafer is then rinsed in the DI water. Finally, the photoresist left on the wafer is stripped off by washing the wafer in acetone. The wafer is then again rinsed in the DI water and dried afterwards.

The processes described in sections 3.4.5 and 3.4.6 are strictly performed in yellow light environment because of the photoresist's sensitivity towards white light. Also, these two processes are repeated in the same order each time a lithographic patterning is to be reperformed.

The wafer is now ready for the anisotropic silicon etching which forms the microstructures in the form of truncated pyramidal pits in the silicon substrate.

5.1.1.7 Anisotropic Silicon Etching

The anisotropic etchant used was PSE-300 ethylene diamine pyrocatechol and water (EDP) produced by Transene Co. Inc.. As shown in fig 5.2, EDP is filled in a beaker and heated to about 100 ^{o}C. A reflux system is placed over the beaker and cold water is circulated through it constantly so that any vapor formed inside the beaker condenses back to the solution, thus maintaining the concentration of the solution through the etching process. The solution was constantly stirred to maintain the temperature of the entire solution. Once the temperature of the solution gets stable at 100 ^{o}C, the patterned wafers are immersed inside the solution. The etching process continues until the etching is over. Since, for this project, a special wafer (SOI), which had an etch-stop layer embedded in it, was used, it wasn't that critically necessary to time the etching process.

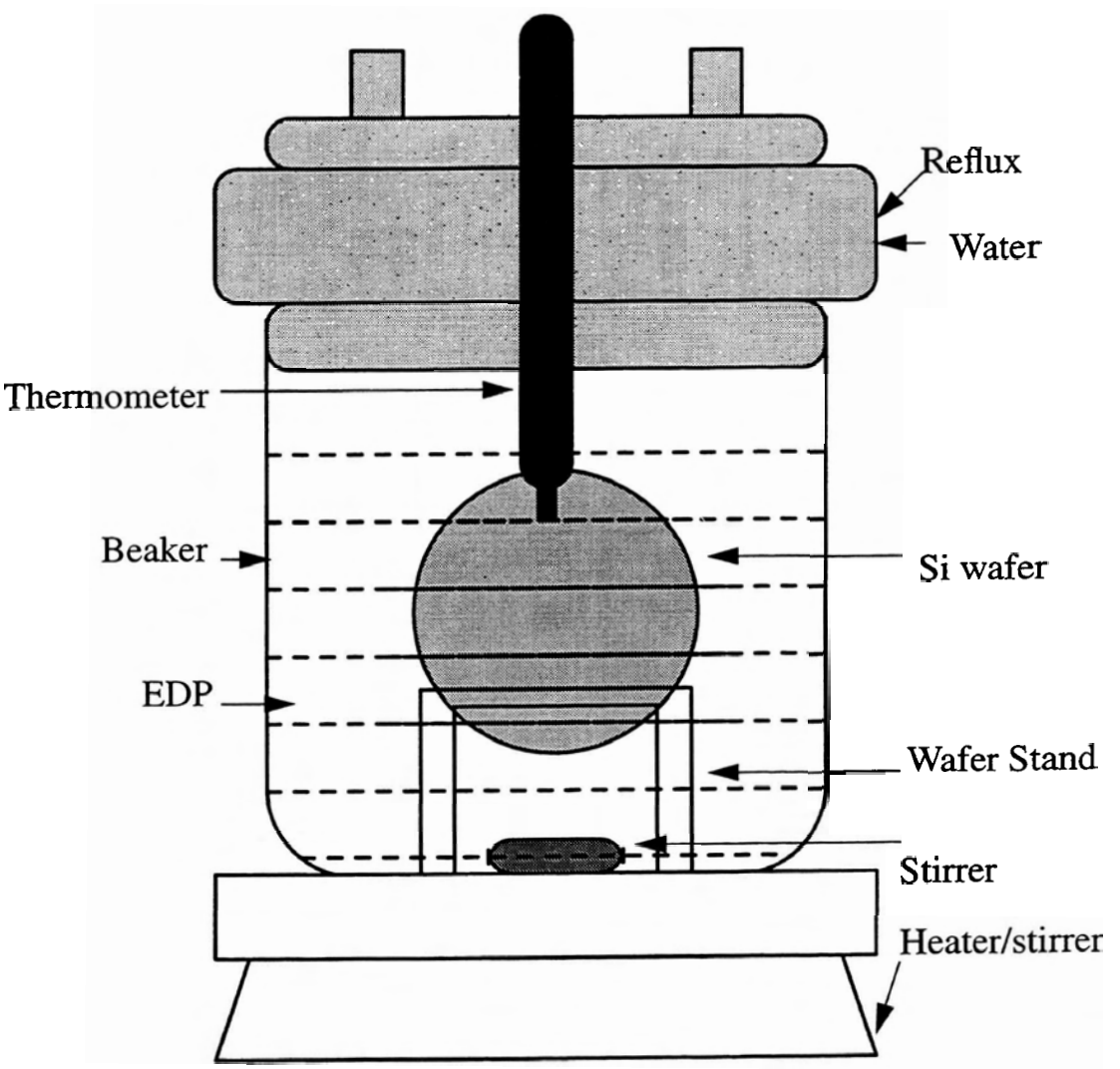

Figure 5.2: Apparatus for Si etching in EDP

To help understanding the etching process better, here are the chemical reactions involved in the process of silicon etching. First, the silicon surface gets oxidized:

$$Si + 2OH^- + 2H_2O \rightarrow SiO_2(OH^-)_2 + 2H_2$$

Then the thin surface oxide is reduced:

$$Si(OH)_4 + 2OH^- + 3C_6H_4(OH)_2 \rightarrow Si(C_6H_4O_2)_3 + 2H_2O$$

EDP, typically, has an etch rate of about 1 μ per minute. Since the wafer's thickness was about 500 μ, the etching process took roughly 8 hours to finish. As a result of the etching process, the truncated pyramidal pits are formed as shown in fig 5.3. The four <111> planes form a slope of 54.74° with the surface of the wafer, <100> plane [13]. The wafer is removed from the EDP solution and rinsed in the DI water very gently and carefully so as not to damage the thin membranes.

Once the membrane was formed, the next step was to form resistors on the top side of the membrane using boron diffusion technique. Before the wafer was inserted into the diffusion furnace, the oxide layer on that side of the wafer was patterned, this time with a diffusion mask. Also, just prior to inserting it into the furnace, the wafer was RCA cleaned to prevent any contamination to the furnace tubes during the subsequent step; diffusion.

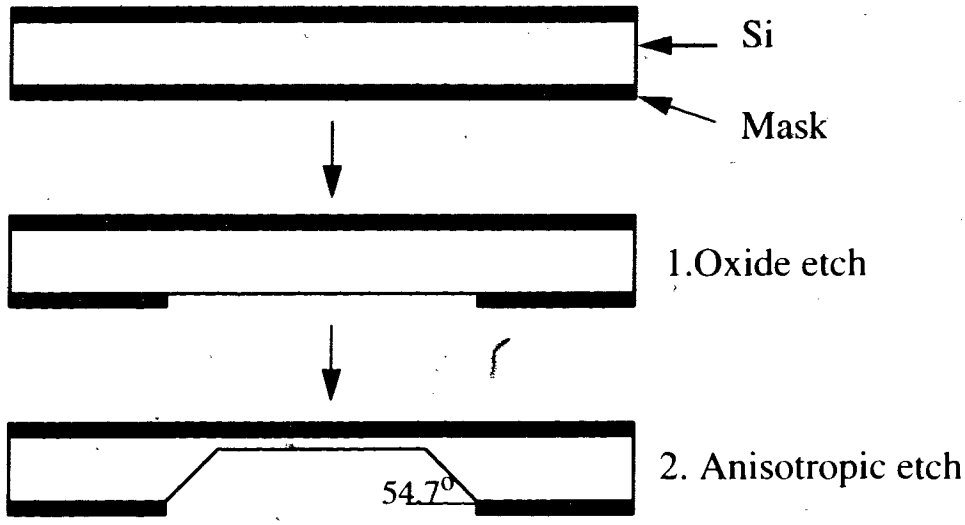

(a)

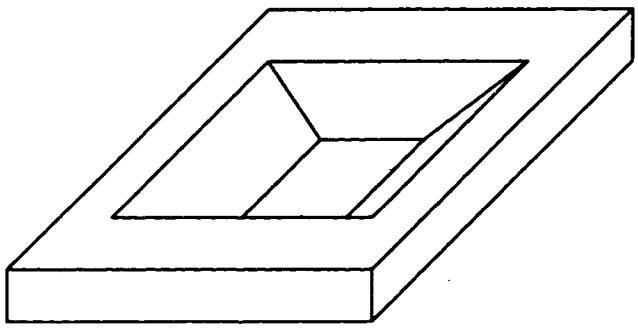

(b)

Figure 5.3: Anisotropic etching of silicon

a) Process steps

b) Isometric view of the etched cavity

5.1.1.8 Diffusion

The piezoresistors in the silicon substrate is made by doping the substrate with p-type material to a depth of about few microns. The process of controlled amount of doping into the wafer is called diffusion. Diffusion is a high-temperature thermal process in which the wafer is placed in a furnace next to the desired dopant source material (boron source for p-type doping) and an inert gas capable of transferring the dopant material at 1100 ^{o}C is passed over the Si wafer-dopant source assembly.

The concentration of dopant material and the depth of diffusion depends upon the duration of the diffusion process. Also, since the resistivity of the doped area depends upon the doping concentration, the desired value of the resistivity can be attained by controlling the duration of the diffusion process. During the process, the diffusion takes place along the depth as well as in lateral directions. To be able to perform the doping in only the selective regions of the wafer, a masking layer on the wafer is required. Similar to the Si etching process, diffusion process also employs silicon dioxide (SiO_2) as the mask material. A thin oxide layer is grown on top of the surface of wafer and exposed regions, for diffusion, in the substrate are created using the lithographic process as described in the previous section. While designing the structure, enough spacing between two diffusion lines is left so that merging between two close adjacent diffusions can be avoided. The diffusion process is illustrated in fig 5.4.

In the boron diffusion process, dopants are usually diffused through a window in a masking layer. Dopant diffusion requires that a dopant source, boron in this case, be placed in intimate contact with the semiconductor wafer surface. Silicon dopants come from either Group IIIA of the periodic table, which form p-type dopants generating excess positive holes, or Group VA, which form n-type generating electrons. Boron (B) was chosen for p-doping in our case.

Boron nitride (BN) which is used as a doping source, is an inert solid material

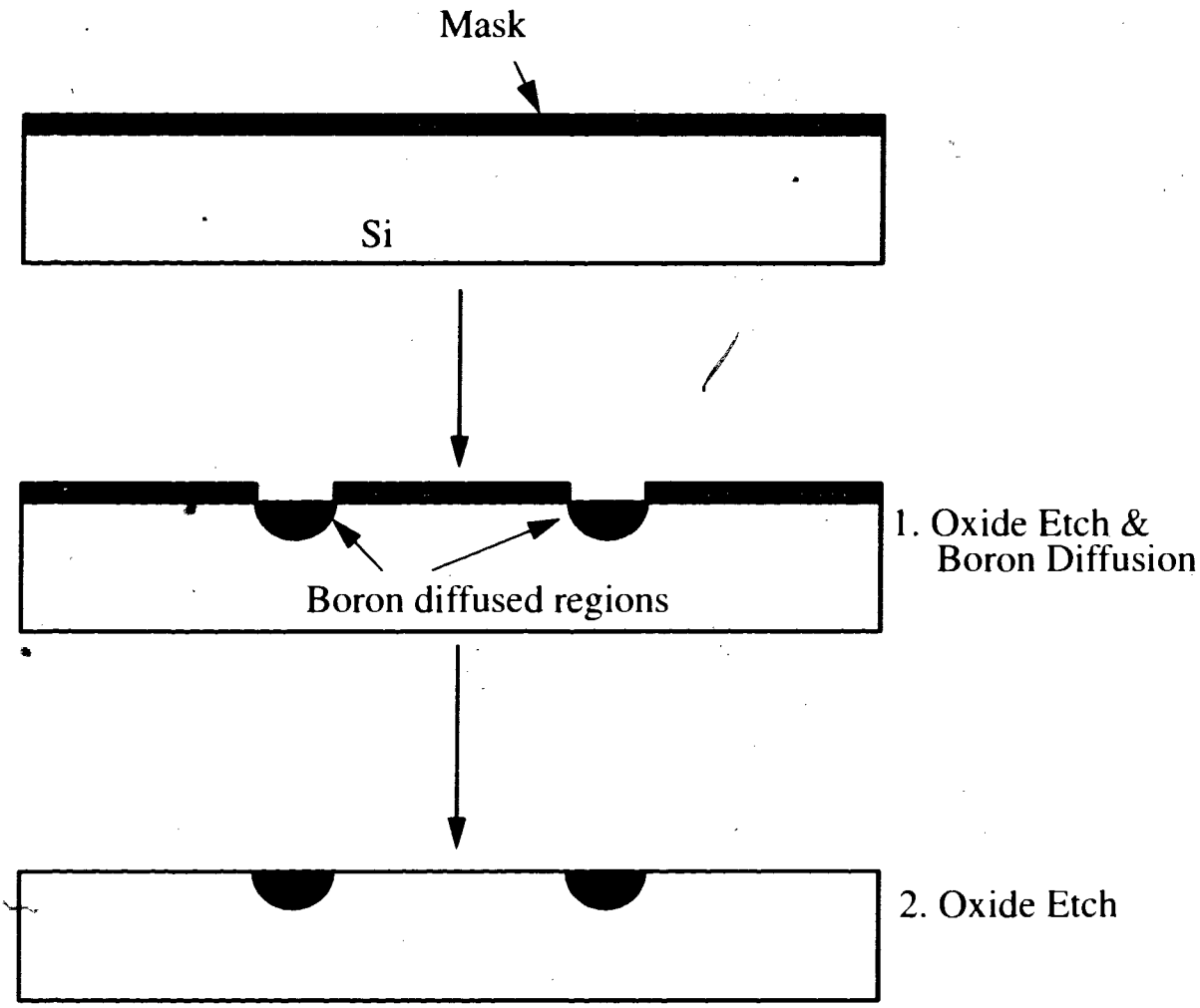

Figure 5.4: Diffusion process sequence

which is machined in the form of a source wafer of the same shape and diameter as silicon wafer being doped. The cleaned wafer with pattern on it was loaded onto the quartzware boat, which is kept in a wafer carrier/loader commonly known as white elephant in semi-conductor process industries. The boron source was kept next to the wafer facing the side of the wafer to be diffused. The wafer was slowly pushed inside the furnace where the temperature was maintained at 1100 ^{o}C. Once the temperature of the furnace reaches stability at 1100^{o}C and in the atmosphere of nitrogen (rate ~ 4 scft), the wafer undergoes the boron diffusion process in the furnace for 30 mins. Under furnace conditions, the BN is

oxidized to form a B_2O_3 glass on the source wafer, this layer then serves to transfer the dopant to the silicon wafer next to it.

$$B_2H_6 + 3O_2 \text{ --> } B_2O_3 + 3H_2O$$

Once the diffusion process was over, the oxide layer was then stripped off by immersing the wafer in buffered HF solution for about 7-8 mins (section 3.4.6). The wafer was then RCA cleaned before putting it in the sputtering chamber for the subsequent process of aluminium deposition.

5.1.1.9 Metallization

This processing step allows the formation of interconnects to the sensors elements on the surface of the wafer. This process is done by Al sputtering.

Sputtering is the phenomenon by which metal conductors can be deposited on the silicon substrate. Plasma, created in the sputtering process, generate a large number of positive ions that are accelerated by the plasma potential and bombard nearby surface. This high energy bombardment causes the atoms of aluminium to get knocked loose thus providing a source of atomized material. The silicon wafer was kept in the sputtering chamber and the pressure was reduced to 10^{-6} to 10^{-8} Torr. The entire wafer was deposited with 1 μ thick Al layer.

The quality of the deposition can be predicted by inspecting the surface of the deposited metal. A good quality sputtering results in the shiny and smooth surface of the metal layer.

5.1.1.10 Aluminium Etching

The aluminium was etched using an aluminium etchant which is a mixture of phosphoric, nitric and acetic acids. The Al layer was first patterned using the metal mask (section 3.4.5 only). The etchant solution was heated to about 50 °C and the patterned wafer was dipped into the solution. The reaction takes place quite vigorously and etches the aluminium in about 1 min or so. The etch rate of the solution at 50 °C is about 100 Å/ sec.

The wafer was rinsed in the DI water and was finally dried. Aluminium etch was the final step of the fabrication processes. In the following section, the bonding technique to bond silicon sensor and glass plate together is described.

5.1.1.11 Spin - On - Glass

To protect the metal pads from corrosion due to exposure of fluid, and also to prevent the electrical current to flow through the fluid due to its direct contact with fluid, a thin layer of insulator (SiO_2) is coated on the wafer. The process is called Spin-On-Glass.

A few drops of Spin-On-Glass solution (ACCUGLASS by Allied Signal Inc.) is dispensed on the wafer surface and the wafer is then spun at 3000 rpm for about 30 seconds. This gives a very thin layer of SiO_2 layer coating on the wafer surface. This thin layer of SiO_2 prevents the electrical current to flow through the fluid.

5.1.2 Anodic Bonding

Generally, one silicon wafer contains many microsensors, in our case about 150 sensors. The processed wafer was scribed and diced in order to separate them and be able

to perform further processing, such as bonding, packaging etc., on them.

After the wafer was diced and each sensor was separated, the back side of the sensor (cavity side) was bonded with a piece of glass. The bonding of silicon and glass is important for the following reasons:

1) To protect the cavity from epoxy material seeping into it during the process of epoxy bonding.

2) To protect the silicon membrane from damage during epoxy bonding or any further processes which may cause a damage to the membrane.

Once bonded with a glass plate, for the pressure sensor to work properly, an opening (or hole) is essential at the center of the glass plate for pressure release. In other words, the cavity underneath membrane should have direct access to the atmosphere in order for the membrane to deflect if pressure is applied from the top side. A hole was drilled at the center of the glass plate prior to anodic bonding.

5.1.2.1 Anodic Bonding

In anodic bonding, the bond is accomplished between a semi-conductive substrate and an ion-rich glass substrate. The silicon and the glass plate on top of each other are placed on the hotplate. The hotplate is heated to ~500 ^{o}C. This temperature is sufficient to make the ions in the glass mobile. When a voltage in the range of ~ 800 Volts is applied between the two substrates with the glass substrate as the anode, the ions are depleted from the glass-substrate interface creating a shallow ion-dependent region about 1 micron thick with high electric field in the order of 7 X 10^{6} V/m. This high electrostatic field pulls the silicon and glass surface close together so that oxygen can move and form new Si-O bonds at the interface. This bonding technique produced a good hermetically sealed bond-

ing between glass and silicon.

Fig 5.5 illustrates the complete fabrication processes discussed in this chapter.

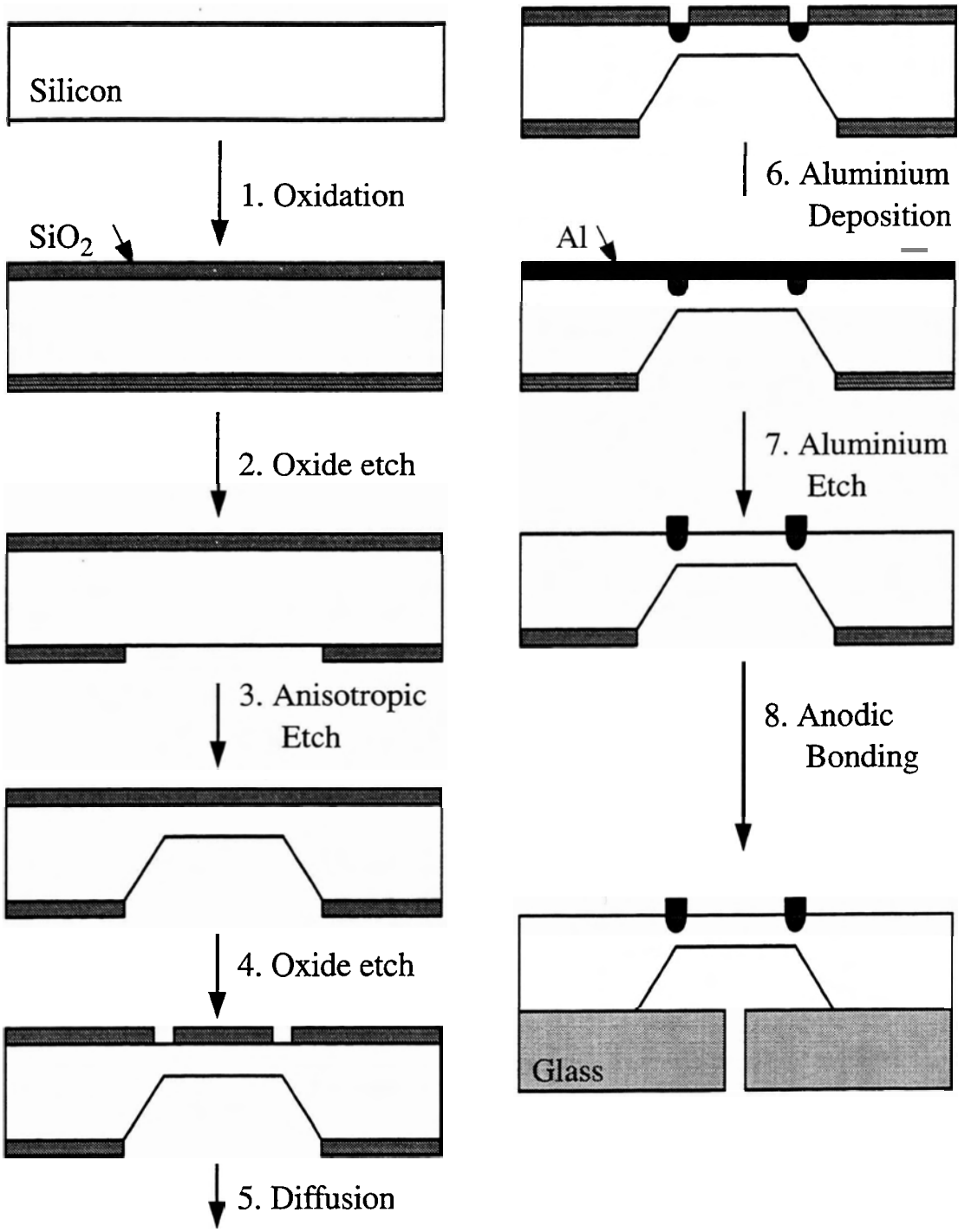

Figure 5.5: Fabrication Process Sequence

5.2 Packaging of the device

This chapter explains the processes involved in assembling and packaging of the sensor. The sensor was packaged using following processes [18]:

1. Anodic Bonding
2. Epoxy Bonding
3. Wire Bonding
4. Tube Fixture

5.2.1 Anodic Bonding

As explained in section 3.5, the silicon part of the sensor is attached with a same size glass piece using anodic bonding technique. The process of anodic bonding is illustrated in figure 5.6.

As shown in above figure, a hole was drilled in the glass plate for the access to the cavity. This access hole facilitates the membrane to deflect when the pressure is applied on the membrane.

5.2.2 Epoxy Bonding

The bonded chip was then attached on to a 40-pin DIP package using a standard epoxy (Epo-tek H70E). Before the sensor chip is bonded on the DIP package, another hole, similar to the one in glass plate, is drilled in the package. This hole also, serving the same purpose, provides an access to the cavity for the deflection of membrane. While gluing, it was made sure that the hole in the package had direct and clear access to the cavity

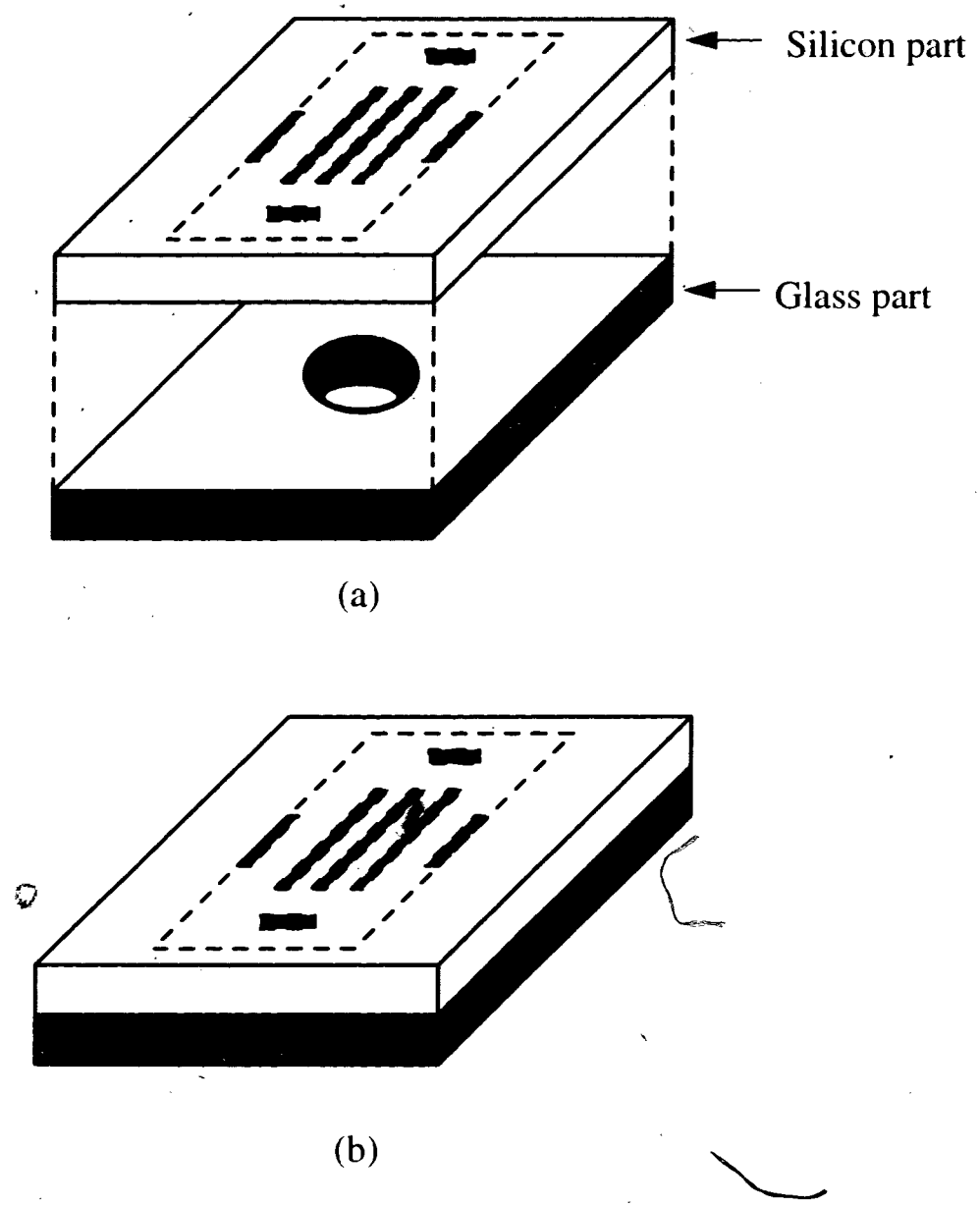

Figure 5.6: Anodic bonding (a) before bonding; (b) after bonding

by positioning the chip properly on the package.

5.2.3 Wire Bonding

The next step was to make the connection between the sensor and the terminals of the package. The electrical connections between the contact pads and package terminals were made by the ball bonding of thin gold wires. Due to the S-O-G layer, it may be necessary to punch through the layer by knocking the bonder tip on it a couple of times in order to be able to make electrical connections.

5.2.4 Tube Fixture

In the last step of assembling and packaging of the device, the device was to be mounted on the wall of a plastic tube. The thought was to mount the device on the wall of a tube so that liquid flow could be in contact with the surface of the device for it to be able to detect the flow rate as well as pressure of the fluid.

To protect the bonding wires from damage due to the fixing of the tube on the sensor, a polymer (EBECRYL 600 : ITA 480 = 7:3 + 0.5% IRGACURE 184) was used. The polymer was dispensed in the empty regions around the chip in the package to cover the bonding wires and, also very carefully, poured onto the Al contact pads of sensor. A sufficient amount of polymer covered all the bonding wires and pads. This polymer was, then, immediately cured with ultra-violet radiation (for 5 mins). The curing of polymer results in the hardening of the polymer thus, securing the wires and bonds from physical damages which may be caused due to the attachment of the tube in the subsequent step.

In the final step of packaging, a square window of appropriate size in 4 mm diameter NALGENE tube was opened. The tube was then fixed on the sensor using a super glue as illustrated in figure 5.7.

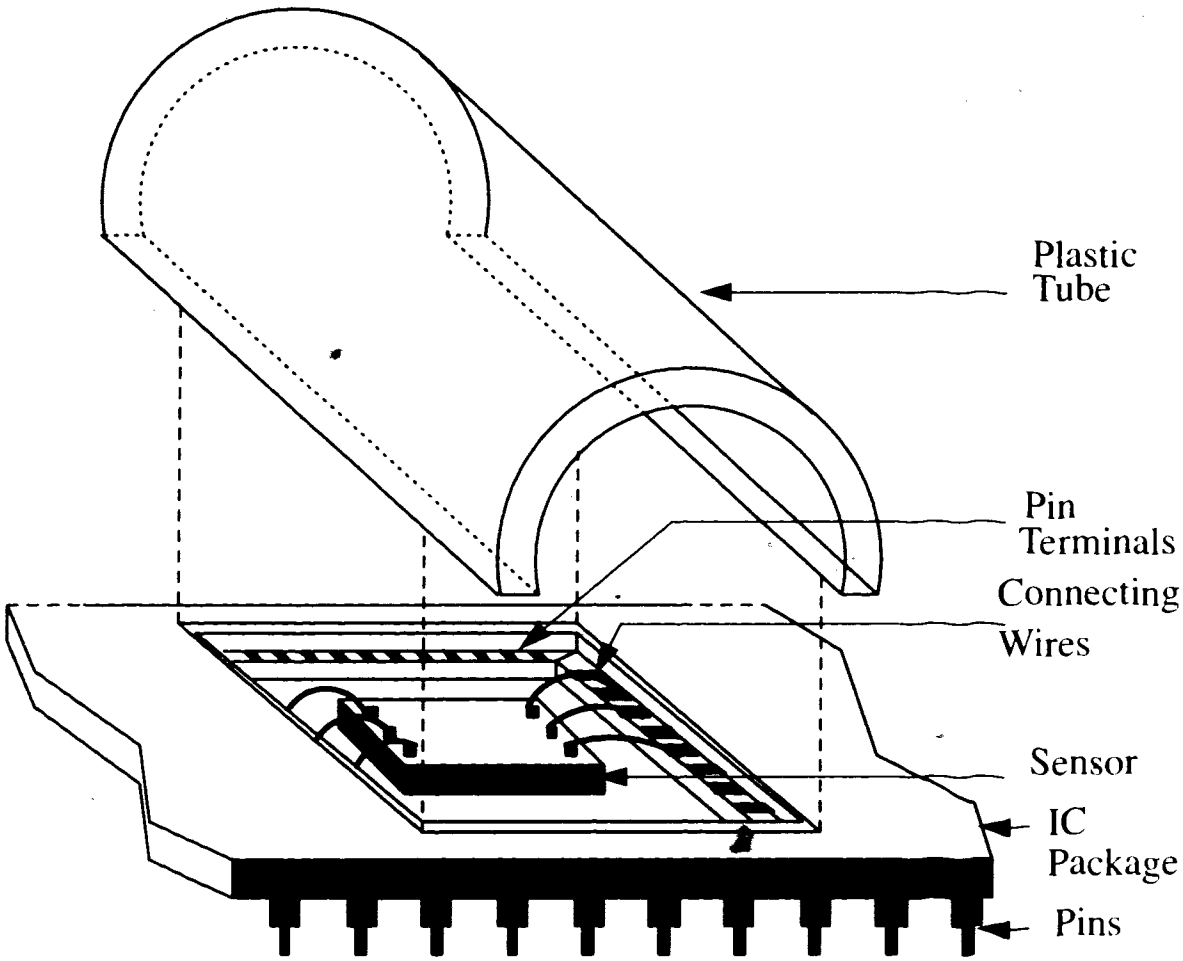

Figure 5.7: The schematic illustration of packaging of the device

In figure 5.7, due to complexity of diagram, only a small portion of tube is shown. A photograph of a final packaged device is shown in figure 5.8.

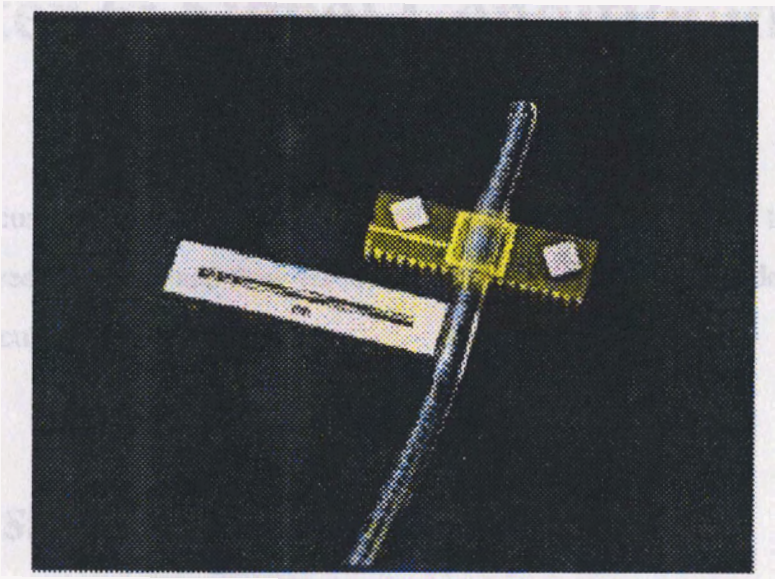

Figure 5.8: Photograph of a final packaged device

Chapter 6: Signal Conditioning Circuit

As discussed in section 4.7, signal conditioning circuit is required to eliminate the cross-talk between pressure and flow sensors. This chapter discusses the design and operation of the circuit.

6.1 Pressure Sensing

This section explains the interference reduction circuit used for pressure sensor [10].

6.1.1 Signal Conditioning Circuit

A common way of achieving high sensitivity and interference elimination is by implementing the Wheatstone bridge measurement method. This method permits the measurement of the voltage difference (or change in current) between two bridge outputs. The circuit used is shown in figure 6.1. Furthermore, it permits an increase in sensitivity and compensates for interference.

R_1 through R_4 are resistors, V power supply and V_o output voltage. Using the notation of figure 6.1, the output voltage, V_o, can be obtained using the following expres

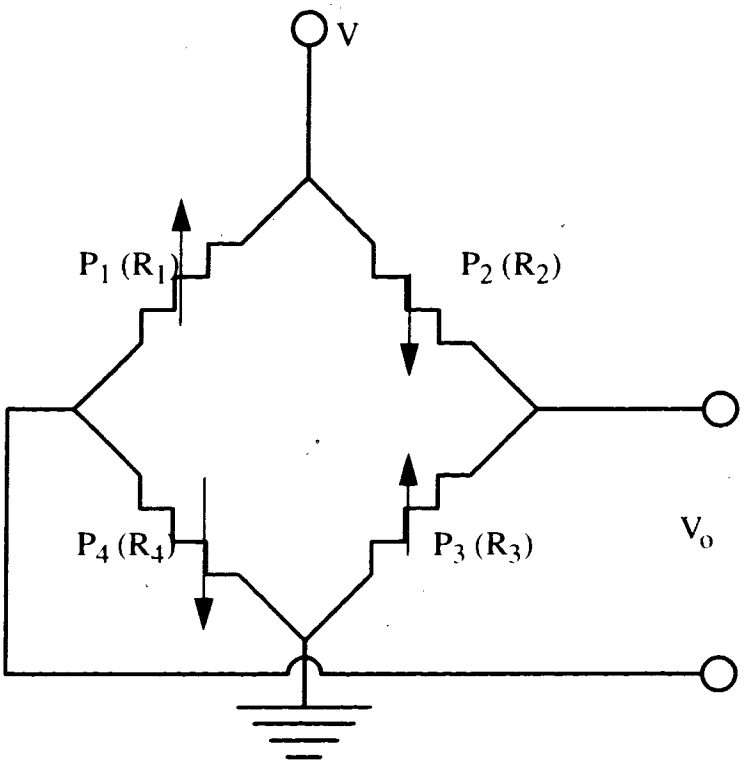

Figure 6.1: Wheatstone Bridge measurement circuit

sion [10]:

$$V_o = V\left(\frac{R_3}{R_2 + R_3} - \frac{R_4}{R_1 + R_4}\right)$$

In this application, four piezoresistors, located on the silicon membrane, are connected in a Wheatstone bridge configuration. This arrangement of pressure measurement method, thus, excludes the use of any external circuit for signal conditioning. Based on the alignment of the piezoresistors with respect to the crystallographic orientation of silicon

planes, R_1 and R_4 are in compressive mode and R_2 and R_3 in tensile mode. As a result, with applied pressure, the resistance of R_1 and R_4 decreases and of R_2 and R_3 increases with the same amount, hence, unbalances the bridge.

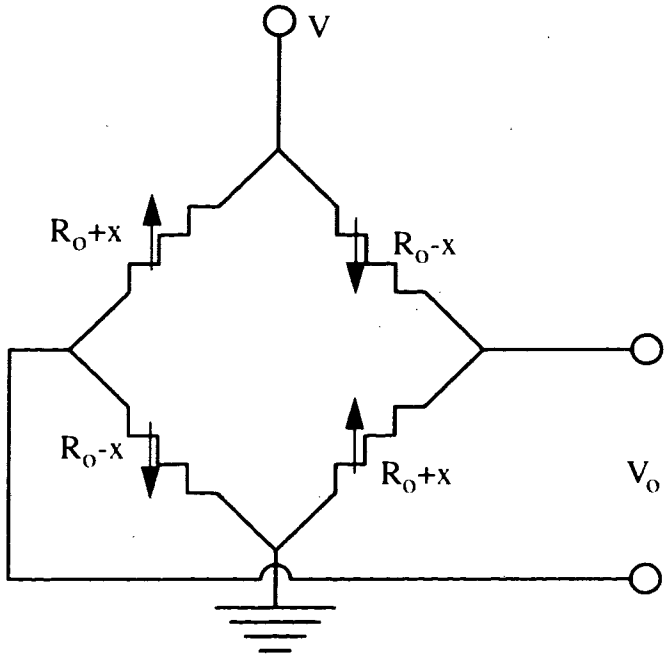

Figure 6.2. Pressure sensors in Wheatstone bridge configuration

R_1, R_2, R_3 and R_4, all, are piezoresistors and they are designed to have the same resistance value at zero pressure (stress), R_o, therefore, the value of their resistances changes when a constant pressure *p* is applied, as shown in figure 6.2:

$R_1 \dashrightarrow R_0 + x$

$R_2 \dashrightarrow R_0 - x$

$R_3 \dashrightarrow R_0 + x$

$R_4 \dashrightarrow R_0 - x$

and the output voltage becomes:

$$V_o = Vx$$

where x is the magnitude of the change of resistance due to a constant pressure p. The above relationship proves that the output voltage of the wheatstone bridge circuit changes proportionally with the change of resistance due to pressure.

This circuit is also used for elimination of interference, due to flow sensor, in the pressure measurement. In this sensor, this noise arises due to the flow sensor, present on the same chip. Flow sensor operates on the principle of heat transfer, which in turn, causes a rise in temperature of the substrate and hence the value of the piezoresistors. A temperature rise in piezoresistors results in change of the resistances. This change in resistances introduces a temperature induced noise in the pressure measurements.

Since all four piezoresistors experience equal change in resistance, due to temperature caused by the operation of flow sensor, the voltage change at two measuring nodes of the Wheatstone bridge are equal in magnitude. The differential voltage measurement method of Wheatstone bridge configuration subtracts these voltage change between two nodes and thus gives interference-deducted output during the pressure measurement.

Assuming y as change in piezoresistors due to temperature, and substituting the following into the expression of output voltage, V_o, (as before $R_1 = R_2 = R_3 = R_4 = R_o$ at zero pressure):

$R_1 \dashrightarrow R_o + y$

$R_2 \dashrightarrow R_o + y$

$R_3 \dashrightarrow R_o + y$

$R_4 \text{ --> } R_o + y$

the expression reduces to:

$$V_o = V\left(\frac{R_o + y}{R_o + R_o + 2y} - \frac{R_o + y}{R_o + R_o + 2y}\right) = 0$$

The above expression shows that the wheatstone bridge output remains unchanged to the effect of temperature on pressure sensor.

6.2 Flow Sensing

A brief discussion on the differential amplifier, used as the signal conditioning circuit for flow sensor, is presented in this section [17].

6.2.1 Signal Conditioning Circuit

A differential amplifier has been used for processing the output signal from the flow sensor. The purpose of the signal conditioner in flow sensing is as follows:

1) To amplify the differential output received from the flow sensor,

2) To eliminate the cross-talk arising due to the pressure sensor.

3) To eliminate the noise due to interference caused by the wire leads.

Differential amplifiers used in a transducer system which produces a relatively small signal, say about 1 mV, between two output terminals are commonly known as instrumentation amplifiers. Instrumentation amplifier is usually used to reject the interfer-

ence signal, from the leading wires, which can sometimes be greater than actual transducer signal, and amplify the small differential signal. As discussed in section 4.5.2, in flow sensing, the difference between two temperature-sensitive resistors is measured. The outputs from these two resistors are fed to an instrumentation amplifier circuit which rejects the interference signal which is common to T_1 and T_2 terminals of the flow sensor and further amplifies sufficiently to be able to detect and display the final output. The circuit for flow sensor is illustrated in figure 6.3

The circuit has three op-amps and consists of two amplifier stages [17]. The first stage is formed by op-amps A_1 and A_2 and their associate resistors, and the second stage is formed by op-amp A_3 together with its four associated resistors.

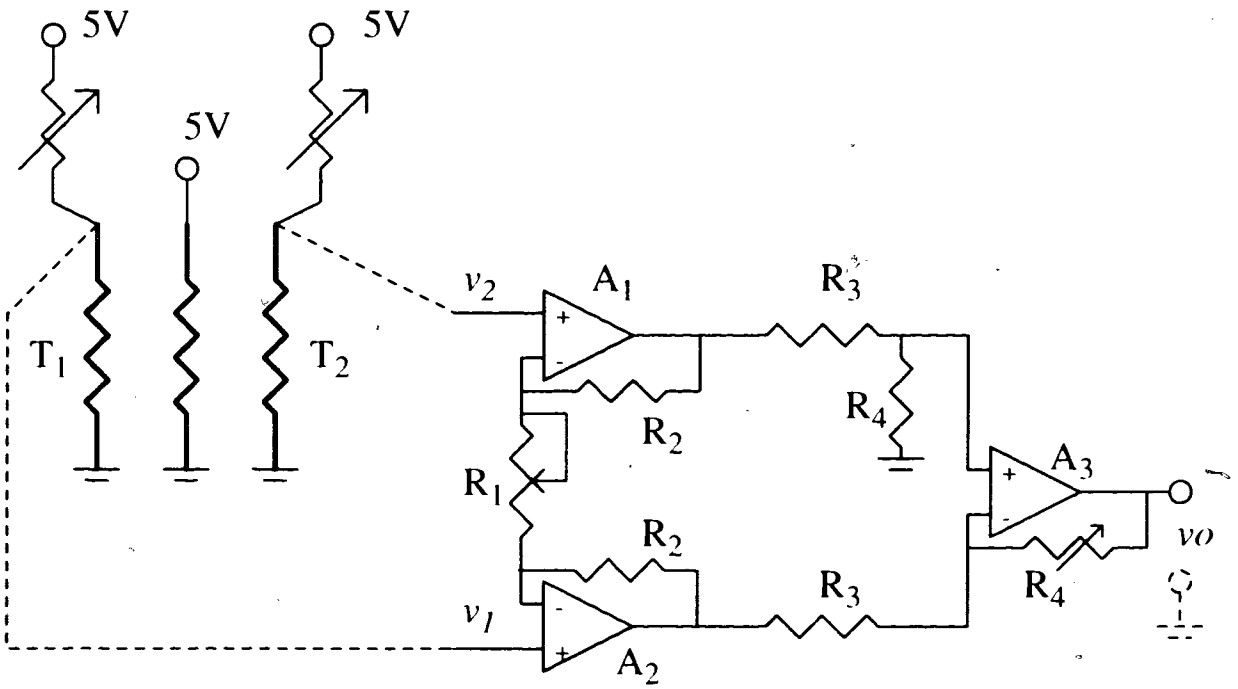

Figure 6.3: Flow sensor with its signal processing circuit

Analyzing the circuit, assuming all three op-amps as ideal op-amps, the expression for overall gain of the circuit can be written as [17]:

$$Gain = \frac{v_o}{v_2 - v_1} = \left(1 + \frac{2R_2}{R_1}\right)\frac{R_4}{R_3}$$

From the gain expression above, the gain value can be varied by varying the single resistor R_1. It is usually preferred to obtain all the required gain in the first stage, leaving the second stage to perform the task of taking the difference between the outputs of the first stage and thus rejecting the common mode interference signal. In other words, the second stage is generally designed for a gain of one. Adopting this approach, we select all range second stage resistors to be equal to a practically convenient value, say $R_3 = R_4 = 10$ kOhm.

Introduction of the variable resistor, R_1, in the first stage, makes it possible to have a variable gain for the first stage amplifier. To obtain the gain range of 2 to 1000, R_1 and R_2 can be calculated and are as follows:

R1 = 100 Ohm

R2 = 50 kOhm

Chapter 7: Testing

Several designs of sensors were fabricated with varying size and thickness (15 - 60 μm) of the membrane and spacing between the flow sensor elements. The spacing *a* and the membrane size *b*, as shown in the appendix B, were varied and are listed in table 7.1. The thickness of the membranes are listed in table 7.2. Experiments were performed separately for pressure and flow sensors. Sensors were first tested for pressure and flow in the air. Sensors were then tested in water.

First, pressure and flow testing were performed using all the devices, designed with various different parameters, to observe the change in performance of sensor with respect to the parameter changes. The result of this testing allowed selecting the design which gave the best output in terms of sensitivity and operating range.

Table 7•1 Different designs of the Sensor

No.	Spacing between Flow sensing elements (μm)	Size of the membrane (μm)
1	25	775
2	100	775
3	100	1325
4	100	1600
5	150	1900
6	150	2500
7	150	3250
8	200	3250
9	250	3250

Table 7-2: Thickness of the silicon membrane

No.	Thickness of membrane μm
1	60
2	30
3	15

7.1 Pressure Sensing

This section explains the experimental setup used in the testing of the pressure sensor. Although in the beginning the experimental setups were changed a few times in order to improvise it, in this section, the setup, which was finally implemented, is presented

7.1.1 Experimental Setup

Input (pressure) was applied at one end of the tube and the other end was blocked using a manual stopper as illustrated in figure 7.1.

At the input end of the tube, the pressure was applied through a pressure gauge so that the pressure gauge (A U-tube with Hg) reading could be used in calibrating the sensor. The output of the pressure sensor was fed to a signal conditioning circuit. The output of the signal conditioning circuit was then visualized and recorded on a HP Semiconductor Parameter Analyzer 4155 A (SPA). SPA was used for monitoring the output as well as power supply to provide the constant current or voltage to the sensor and the circuit.

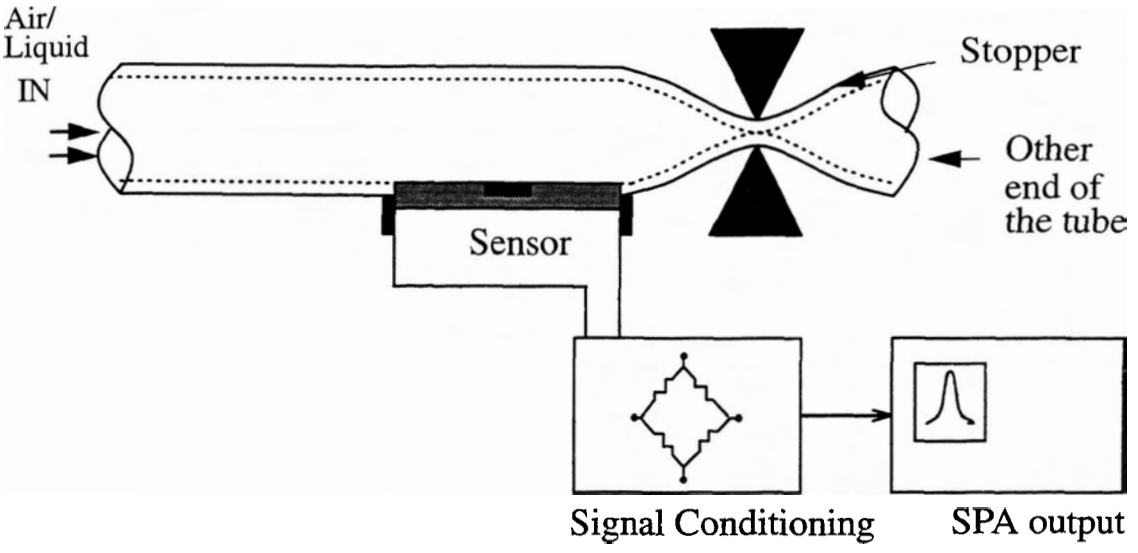

Figure 7.1: Experimental setup for pressure sensor

7.2 Flow Sensing

This section explains the experimental setup used to test the flow sensor in the laboratory.

7.2.1 Experimental Setup

Fluid was passed through the tube in a setup as illustrated in figure 7.2. Extreme care is taken in ensuring that the least turbulence is created in the flow of the fluid during the measurement. The output from the flow sensor is fed to a signal conditioning circuit for signal processing and the final results are displayed and stored in the SPA machine. The flow sensor was calibrated using a standard flow meter (Matheson 603), connected in series with the fluid line. Alternatively, the input flow rate, for calibration purposes, can

also be found out by measuring the volume of dispensed liquid at the output end with respect to time.

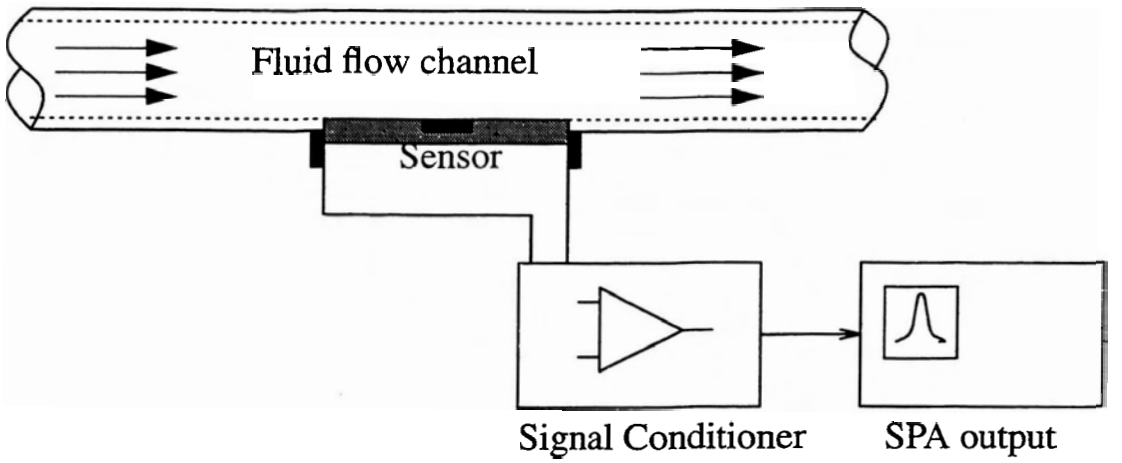

Figure 7.2: Experimental setup for flow sensor

Chapter8: Results and Discussion

8.1 Results

Devices were tested for pressure and flow, first, in air and, then, in liquid medium. Initially, as listed in table 5.1 and 5.2, the devices with thicker membrane (60 μm) were fabricated and tested. These devices had extremely low sensitivity and a very limited range of measuring pressure and flow. These problems were due to the fact that the membranes were too thick.

In the next batch of the fabrication, the devices with membrane thickness of 30 μm were fabricated. Although, these devices showed an improved sensitivity and operating range for pressure, the sensitivity for the flow sensor was still poor. Due to a thicker membrane, the power consumption in operating the heater (for flow sensor) was very high as well.

Finally, devices with even thinner membranes were fabricated. Using an SOI wafer, it was possible to successfully fabricate the devices with a 15 μm thick membrane. These devices, in conjunction with a signal processing circuit, exhibited excellent sensitivity and operating range for both pressure and flow sensor. The power consumption was reasonably low as well.

In this section, the results associated with the preliminary testing of the devices, in the liquid medium, are presented.

8.1.1 Pressure sensor

The device was first calibrated for the pressure sensor. The pressure sensor was

tested for a pressure range of 0 - 78 cm of Hg in the water medium. The output voltage from the Wheatstone bridge was plotted with respect to the pressure applied. The response is shown in figure 8.1.

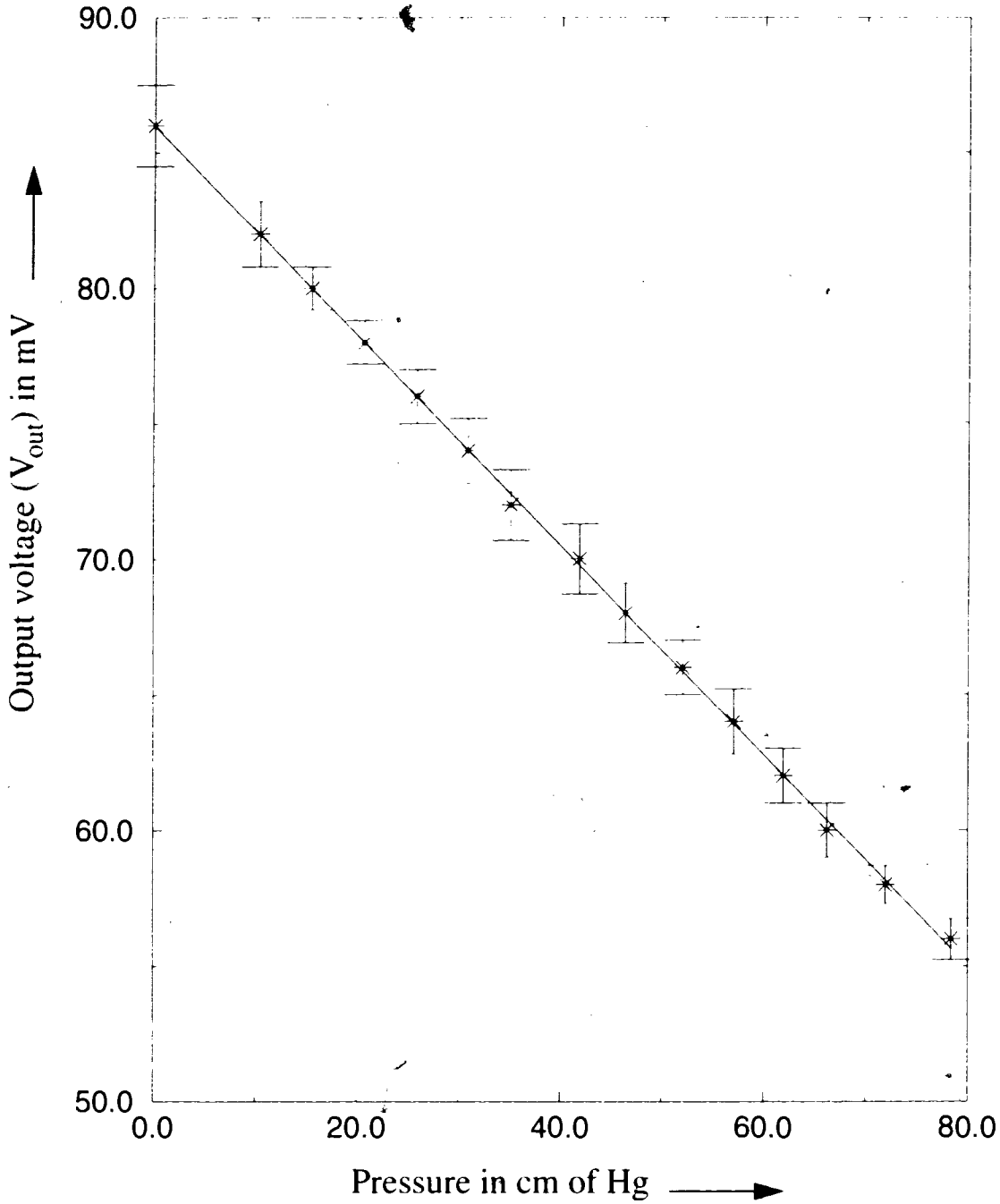

Figure 8.1: Response curve for pressure sensor [18]

Experiments were performed to investigate the interference, arising due to the flow sensor, during the pressure measurement. The flow sensor causes an increase in temperature of the chip which, subsequently, affects the piezoresistors and introduces temperature-induced interference in the pressure measurement.

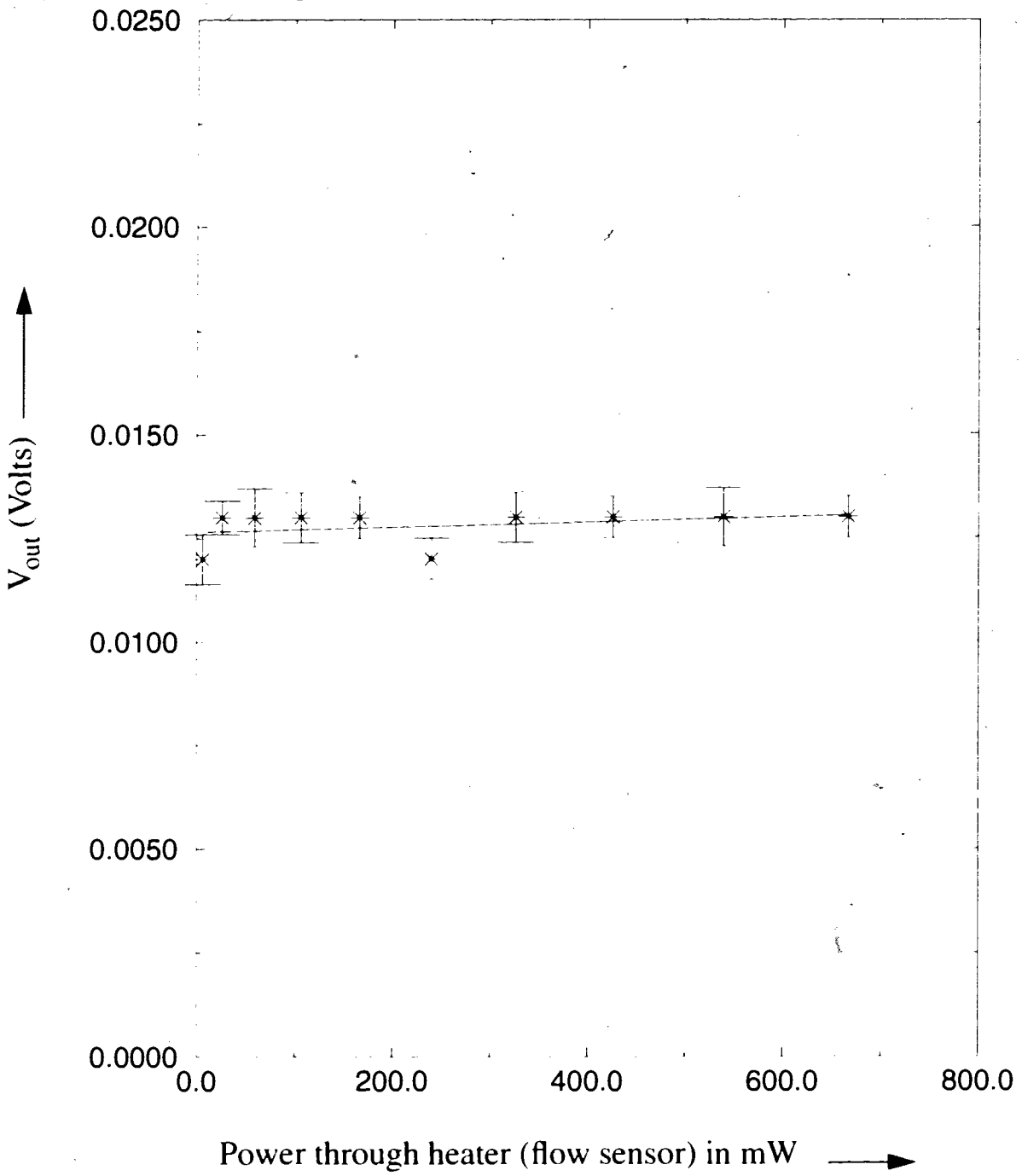

Figure 8.2: Effect of heat on pressure measurement [18]

To investigate this noise, the flow sensor was powered with a range of input voltage and the Wheatstone bridge output for pressure sensor were recorded. Alternatively, this experiment could be done by placing the sensor in an oven which could be programmed for the desired temperature range.

Based on the data from above experiment, a graph was drawn between bridge output and the power supplied to the heater element of flow sensor. The graph is shown in figure 8.2.

8.1.2 Flow Sensor

The flow sensor was first calibrated for a flow range of 0 - 45 ml/sec in the water medium. The output from the two temperature sensitive resistors (flow sensor) is fed to the differential op-amp circuit and the final differential output voltage was recorded against the flow rate. The response is shown in figure 8.3.

In the next phase of the experimentation, the introduction of interference due to the presence of pressure was investigated. A deflection in the membrane, due to liquid pressure, can cause a change in the resistance of temperature sensitive resistors and hence can add an interference in the flow measurement.

The differential measurement method using the op-amp circuit, as a signal processing circuit, cancels out this effect of membrane deflection on flow measurement and gives the flow response which is free of any interference arising from pressure sensor. The result is illustrated in figure 8.4.

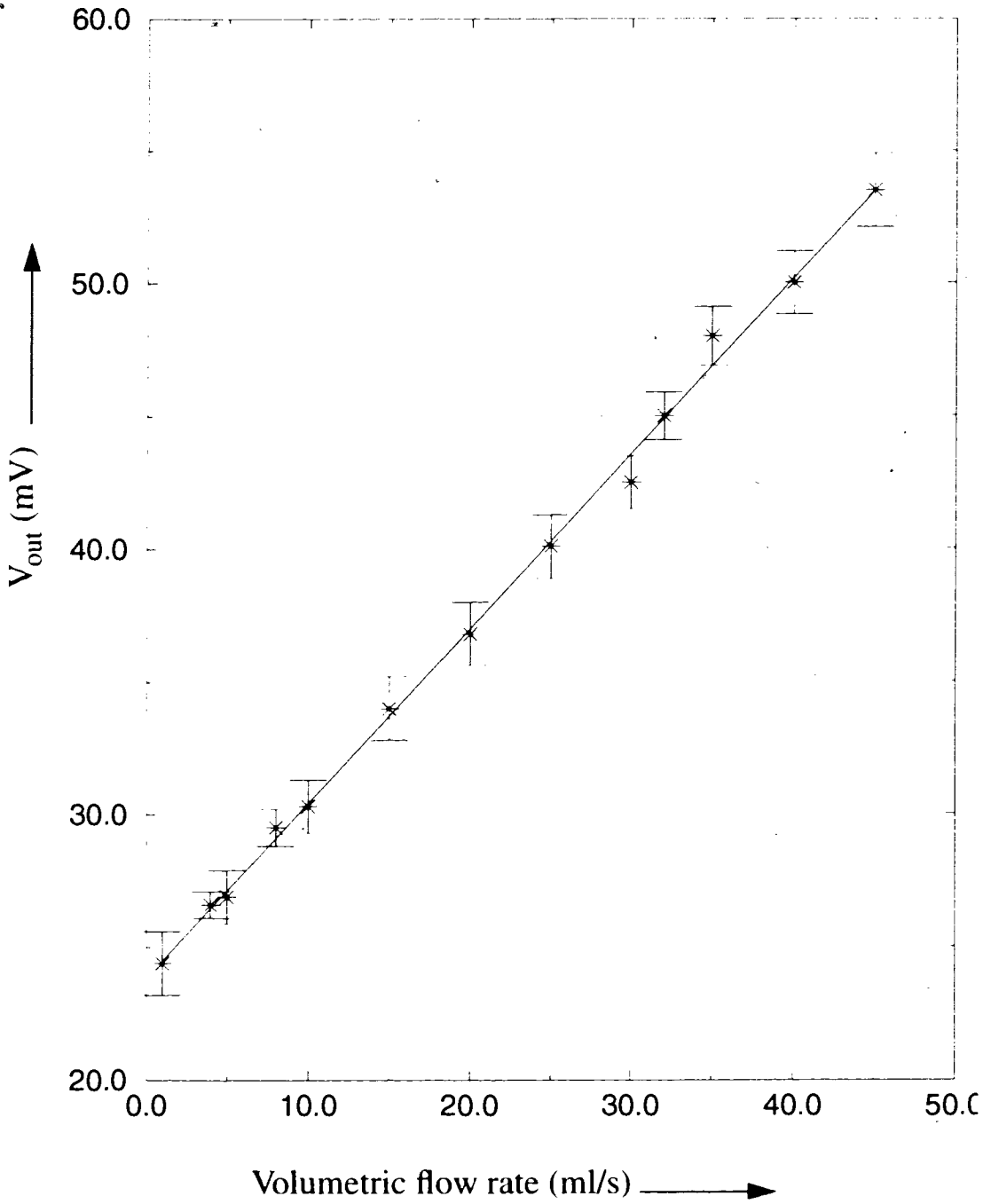

Figure 8.3: Response curve for the flow sensor [18]

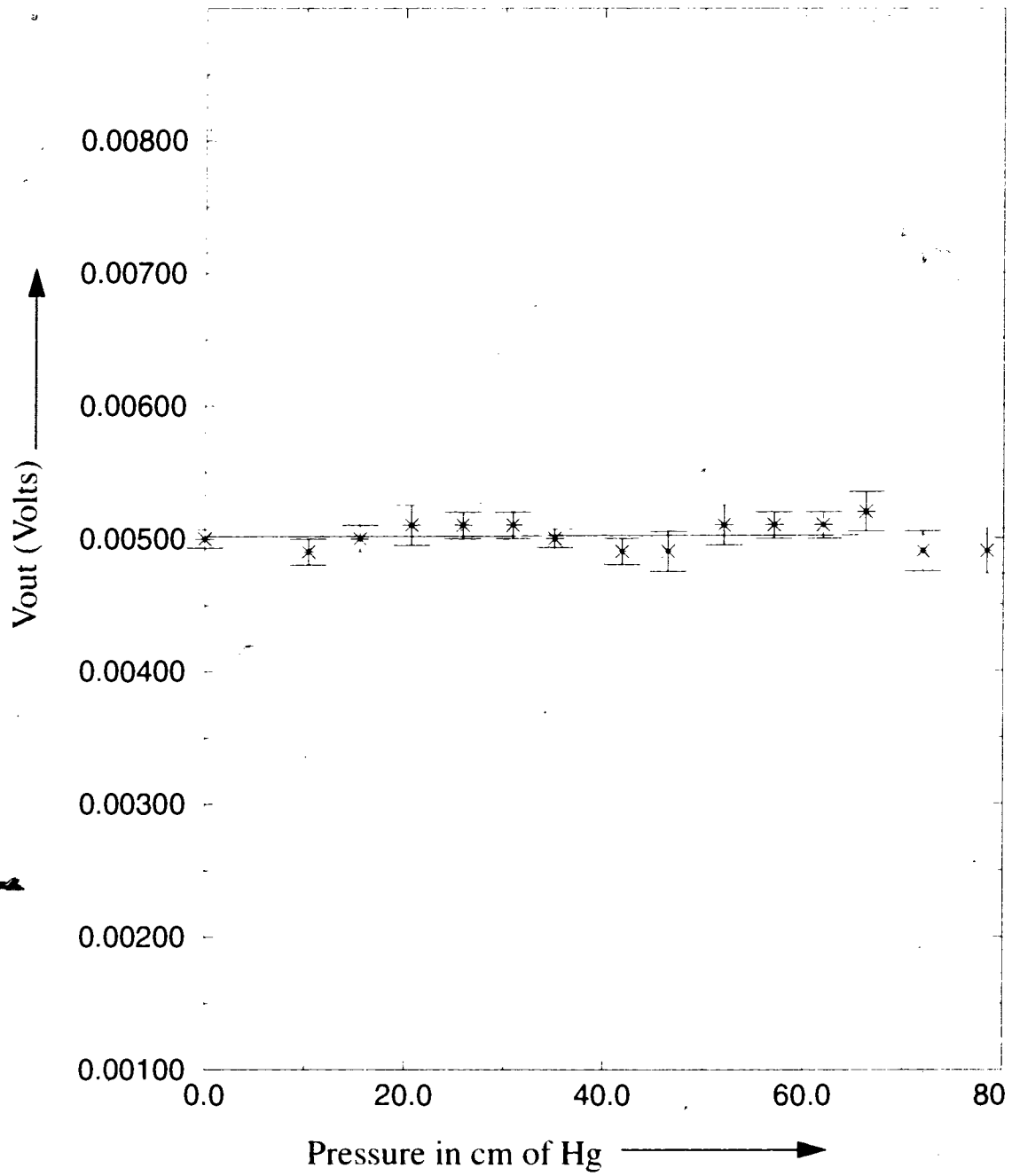

Figure 8.4: Effect of pressure on flow measurement [18]

8.2 Time Response of the Flow Sensor

The time response of the flow sensor was recorded and is illustrated in figure 8.5.

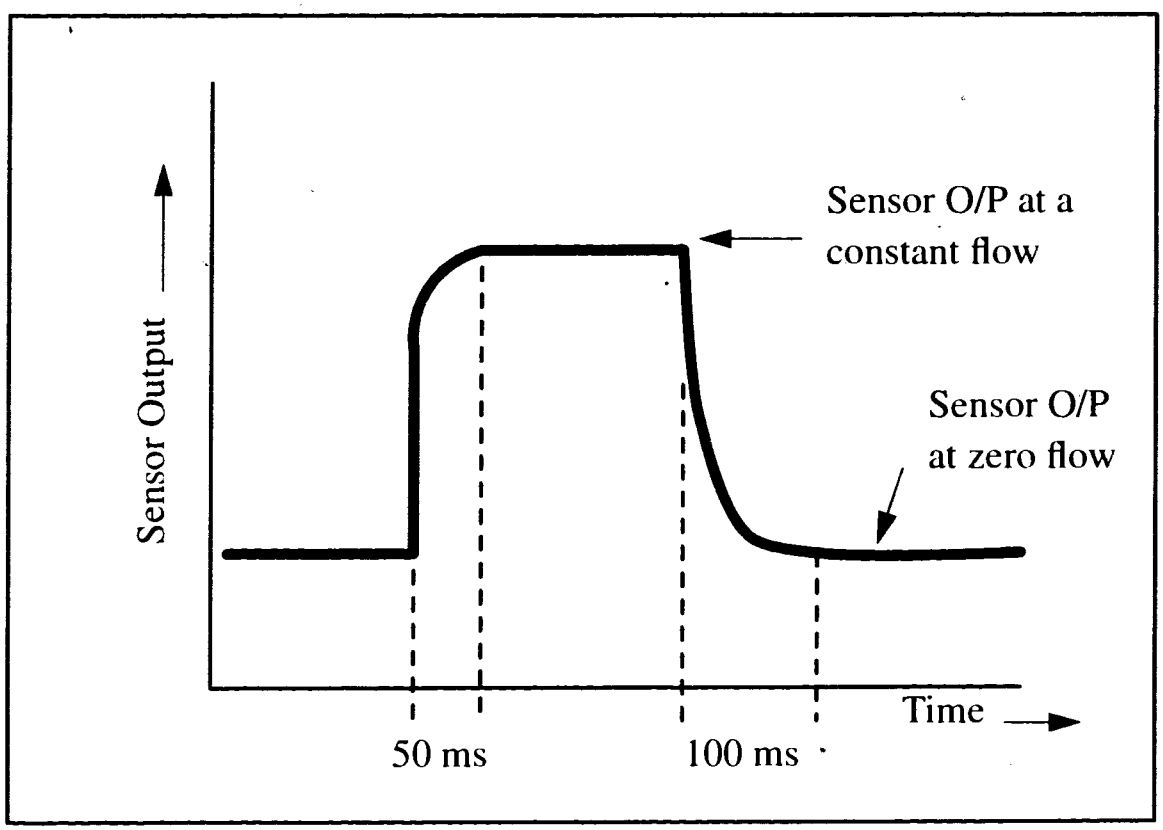

Figure 8.5: Illustration of time response of the flow sensor

The rise and fall of an output signal from the sensor is:

τ_{rise} = 50 ms

τ_{fall} = 100 ms.

8.3 Discussion

Figure 8.1 illustrates that response of the pressure sensor shows linearity for the range of 0 to 78 cm of Hg and offers a high pressure sensitivity of 1 mV/10 mm of Hg. Use of Wheatstone bridge method makes an easy and effective way to eliminate the interference from flow sensor in pressure measurement (figure 8.2).

Also, the sensitivity (0.89 mV/(ml/s)) and dynamic range (0 to 45 ml/s) of flow sensor, and its ability to work in the fluidic medium makes it an excellent candidate for its application in the prostate cancer detection. The differential amplifier circuit used as a signal conditioning circuit in flow sensing gives an interference-free output.

Both pressure and flow sensor have a time response of 50 ms.

Both pressure and flow sensor utilizing thin film diaphragms offer high sensitivities over wide dynamic ranges. Cross-talk was easily eliminated using asignal conditioning circuit. Both sensors utilize integrated-circuit batch-processing techniques and are potential solutions to high-volume low-cost applications. For both types of sensors, diaphragm thickness is the structural parameter requiring the greatest control. This was achieved by the use of a etch-stop silicon wafer (S-O-I Wafer) to stop the etching in order to obtain a uniform thickness of diaphragm.

Chapter 9: Conclusion and Future Work

9.1 Conclusions

A novel application of micromachined pressure-flow sensor in the field of biomedical sciences has been demonstrated in this thesis. Pressure and flow sensors based on Bulk Micromachining Technology were employed as the sensors to evaluate bladder pressure and urinary flow rate in order to diagnose an early detection of prostate cancer. The pressure sensor, based on piezoresistive effect, worked on the principle where a deflection of the membrane causes a stress in the piezoresistors and hence, a change in resistors. Moreover, the operation of the flow sensor was based on the principle of heat transfer in anemometry method. This thesis presents a sensor system which has pressure and flow sensors integrated together on one single silicon chip to help in diagnosing the detection of prostate cancer.

Sensors were fabricated on top of a 15 μm thick silicon membrane, using an SOI wafer, formed by anisotropic etching of silicon. Devices were enclosed in a 40-pin Dual-In-Line IC package and properly packaged to mount the device on the wall of a plastic tube. The device is packaged such that detection of prostate cancer can be performed non-invasively. Sensors were tested in the laboratory for pressure and flow rate in the liquid medium.

Simple electronic circuits were employed to process the output signals for these sensors. These circuits were also designed to successfully eliminate the cross-talk between pressure and flow during their operation.

The required pressure and flow range for the detection of bladder pressure and uri-

nary flow rate were as follows:

1) Pressure range: 0 - 150 mm of Hg

2) Flow range: 0 - 25 ml/sec

The results associated with the preliminary laboratory testing of sensors are as follows:

1) Pressure range: 0 - 78 cm of Hg

2) Pressure sensor sensitivity: 1 mV/ (10 mm of Hg)

3) Flow range: 0 - 45 ml/sec

4) Flow sensor sensitivity: 0.98 mV/(ml/sec)

The testing of the sensors in the saline water medium proves that there was no significant effect of electrical conductivity observed in the operation of the sensors, hence, making these sensors quite suitable for operating in urine medium to evaluate bladder pressure and urinary flow rate.

9.2 Future Work

This thesis describes the preliminary results of testing of the sensors in the laboratory. After obtaining the successful laboratory results, the devices have been scheduled for clinical testing at Urology department of The Vancouver General Hospital (VGH). In order to perform the clinical testing, the packaging of the device would have to be adequately modified such that the actual proposed method of non-invasive measurement of bladder pressure and urinary flow rate could be complied. The modified version of the packaging incorporates a stopper, mechanical or electronic, which could facilitate the bladder pressure just before the voiding and also during the voiding. It is to be made cer-

tain that the stopper, whether operated mechanically or electronically, must block the urine flow only for a very brief period of time so that this forced blockage doesn't cause any change in the urine flow pattern subsequently.

9.3 Other Applications

Integration of pressure and flow sensors together in a single silicon substrate and the reduced size of the sensors fabricated using silicon micromachining technology have opened the door to many other applications, particularly in the field of biomedical sciences where the measurement of fluid pressure as well as flow in an artery becomes an immediate demand. One such example is the use of pressure and flow sensors in Live Organ Carrier/Preservation systems (LOCS), commonly used for the Kidney transplant and procurement. In order to preserve a donor organ (kidneys), a kidney preservation solution is constantly pumped into the organs in a pulsatile mode. To make certain that the organ is functioning well during the transportation of the organ, a constant check on the pressure, flow and temperature of the solution is highly required.

The pressure-flow sensor, described in this thesis, matches very well with the requirements of the sensors which can be used in this system to provide pressure in the organ while the solution being perfused and flow rate of the solution, perfusing into the organ. The device can, easily, be incorporated in the LOCS and the pressure and flow rate of the solution can be recorded and, also, visualized on a display screen. This sensor design is also capable of introducing a temperature sensor, T_1 and T_2, and integrating it together with existing pressure-flow sensor, thus, providing all three pressure, flow and temperature of the solution in the live organ carrier system. The proposed design of integration of a temperature sensor in the existing pressure-flow sensor is shown in figure 9.1.

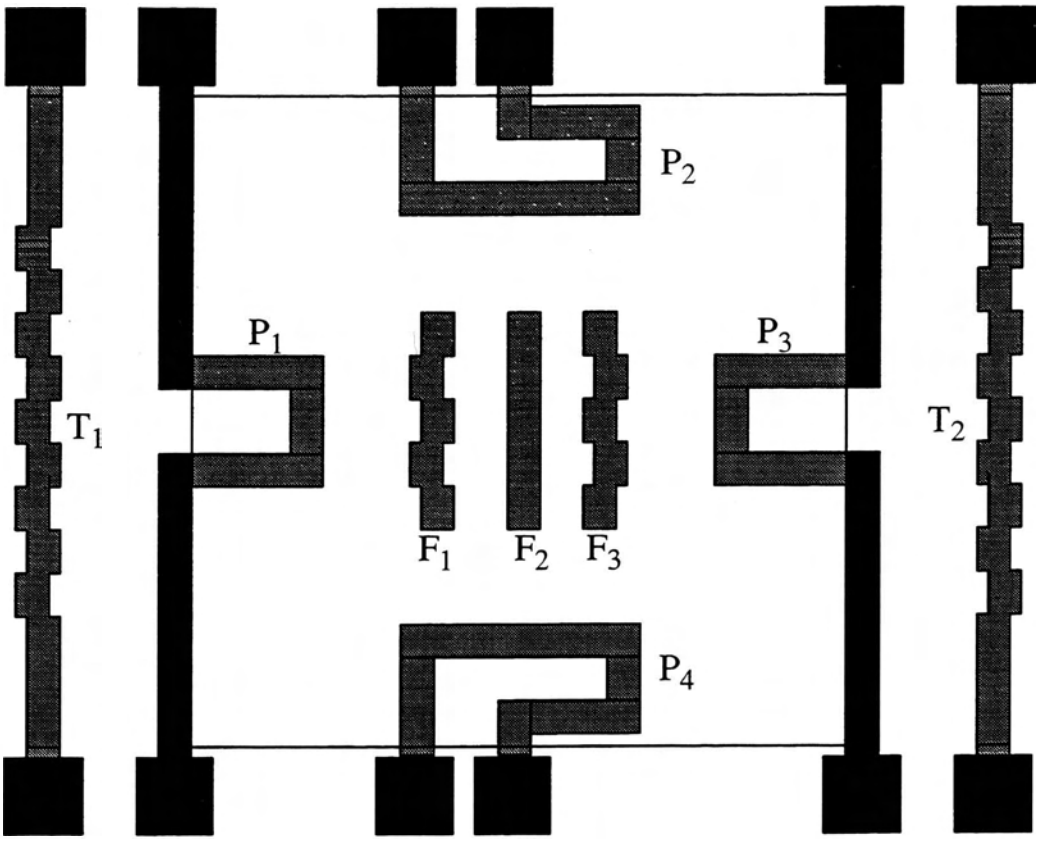

Figure 9.1: Proposed design of integration of temperature sensor with pressure-flow Sensor.

F_1, F_2, F_3 ----> Flow Sensor

P_1, P_2, P_3, P_4 -> Pressure Sensor

T_1, T_2 --------> Temperature Sensor

APPENDIX A: Sensor Layout Designs on Mask Plates for Fabricating the Sensors

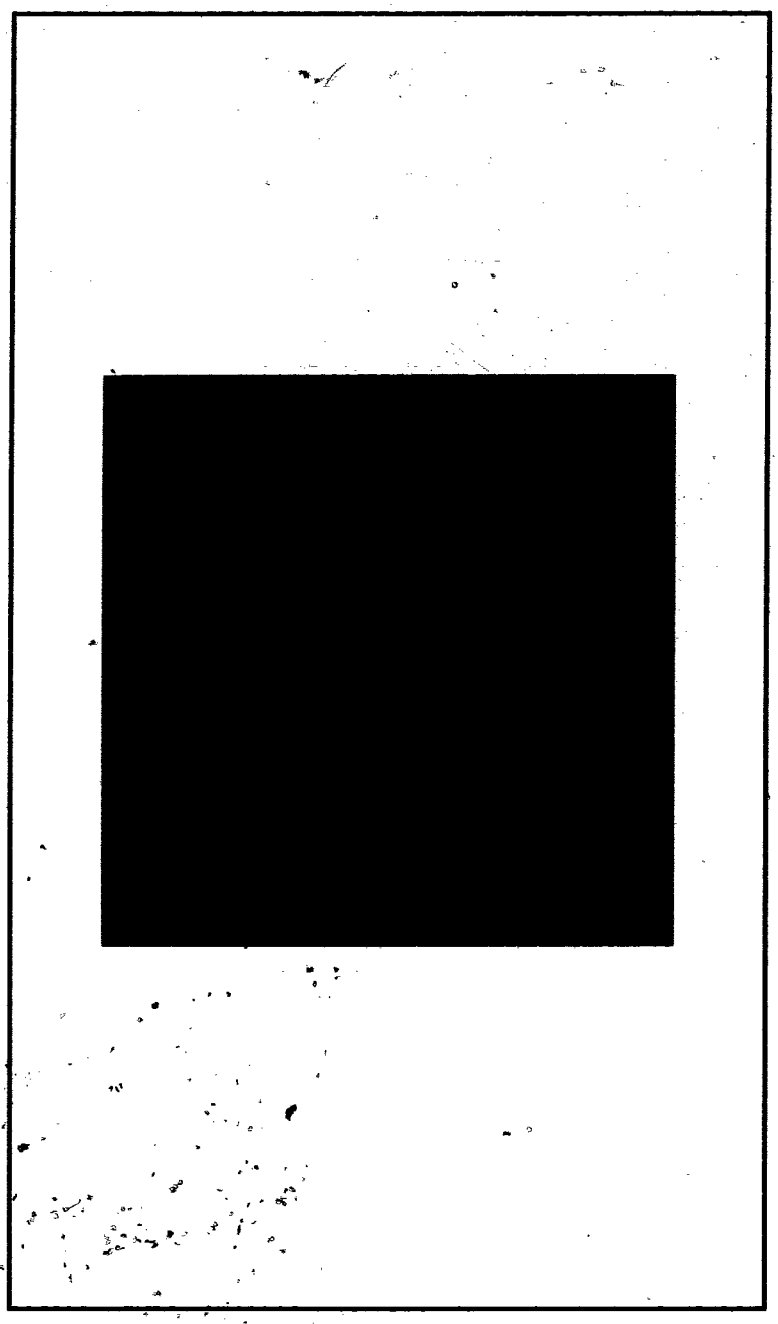

Figure A-1: Mask Design for Silicon Anisotropic Etching

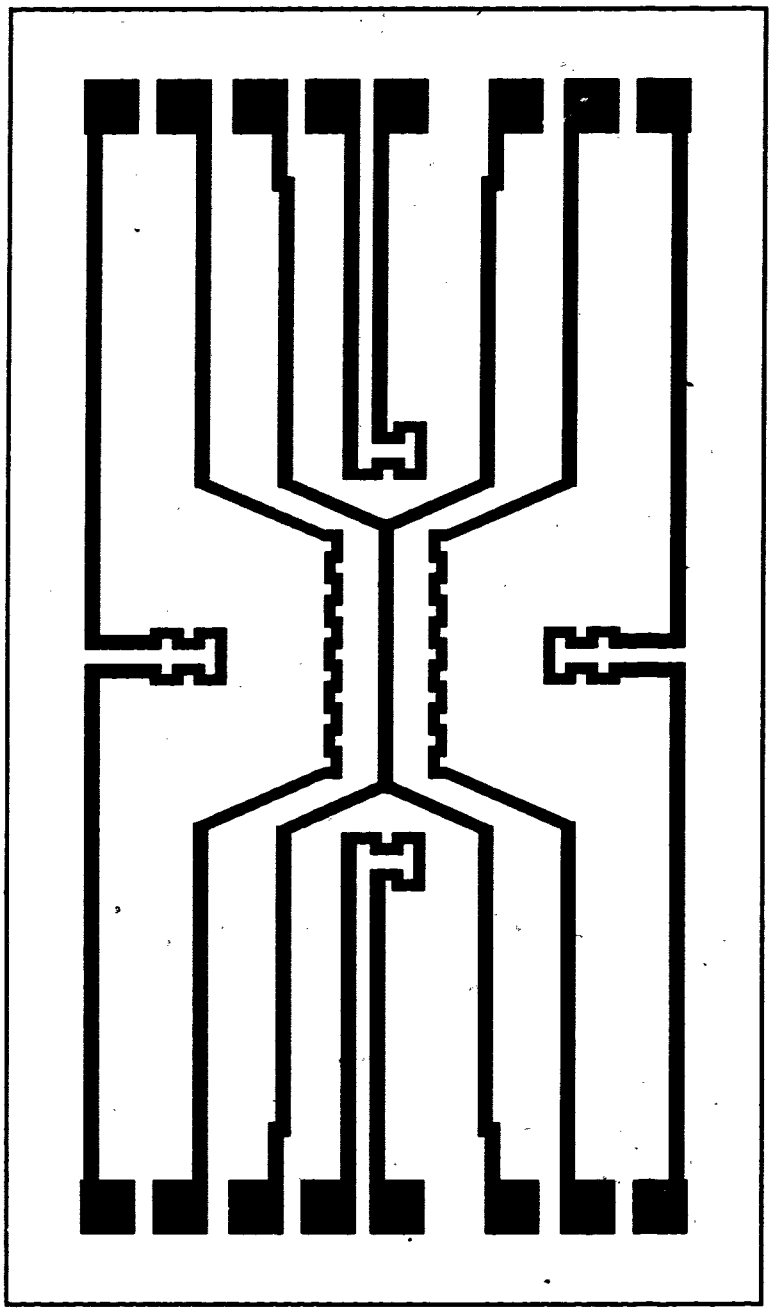

Figure A-2: Mask Design for Boron Diffusion

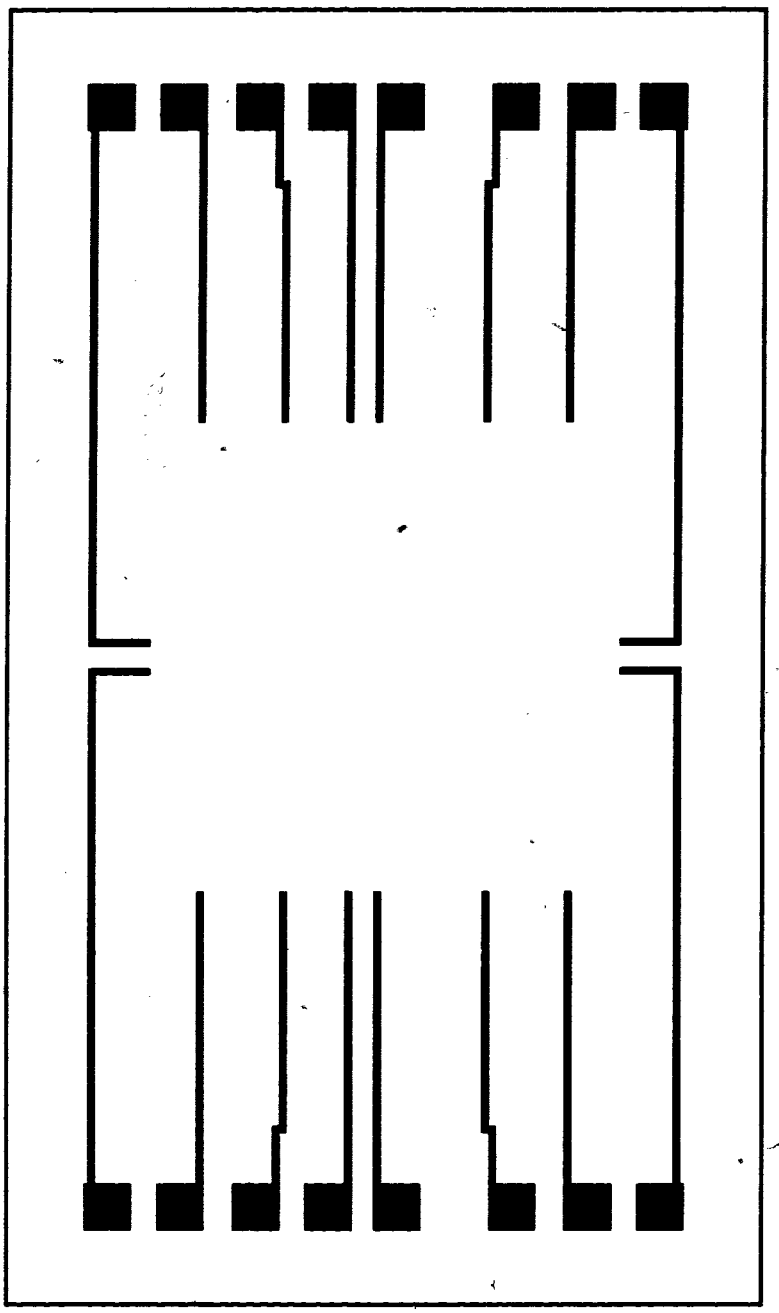

Figure A-3: Mask Design for Metallization

LIST OF REFERENCES

[1] Greg Paula, "MEMS Sensors", IEEE, Transaction of Mechanical Engineering, Vol. 118, No. 10, Oct. 1996.

[2] M.Mehta, "A Micromachined Capacitive Pressure Sensor for use in Endoscopic Surgery", M.A.Sc. Thesis, Engineering Science, SFU, 1995.

[3] Anders Spanberg and et. al., "Pressure/Flow Studies Preoperatively and Postoperatively in Patients with Benign Prostatic Hypertrophy", Neurology and Urodynamics 10:139-167 (1991).

[4] M. Tojo and et. al., "Relationship between Bladder Neck Diameter and Hydraulic Energy at Maximum Flow", The Journal of Urology, Vol. 152, 144-149, July 1994..

[5] Werner Schafer, "Principles and Clinical Application of Advanced Urodynamic Analysis of Voiding Function", Urology Clinics of North America, Vol. 17, No. 3, August 1990.

[6] S. J. Lammerink, "Micro-Liquid Flow Sensor", Sensors and Actuators, A, 37-38, 1993, 45-50.

[7] M. Akbar, "Temperature Compensation of Piezoresistive Pressure Sensors", Sensors and Actuators A, 33, 1992, 155-162.

[8] S. Bouwstra, "Resonating Microbridge Mass Flow Sensor", Sensors and Actuators, A 21-23, 1990, 332-335.

[9] C. Yang, "Monolithic Flow Sensor for Measuring Millilitre per minute Liquid Flow", Sensors and Actuators, A 33, 1992, 143-153.

[10] Duane Tandeske, "Pressure Sensors - Selection and Application", Mercel Dekker, Inc., 1990.

[11] S. K. Clark, "Pressure Sensitivity in Anisotropically Etched Thin-Diaphragm

Pressure Sensors", The Transactions of Electron Devices, Vol. ED-26, No. 12, Dec 1979.

[12] K. E. Peterson, "Silicon As a Mechanical Material", Proceedings of the IEEE, Vol. 70, No. 5, May 1982.

[13] J. W. Gardner, "Microsensors - Principles and Applications", John Wiley and Sons, 1994.

[14] S. Middelhoek, S. A. Audet, "Silicon Sensors", Academic Press, 1989.

[15] S. M. Sze, "Semiconductor Sensors", John Wiley and Sons, Inc., 1994.

[16] L. Ristic, "Sensor Technology and Devices", Artech House, 1994.

[17] A. S. Sedra, K. C. Smith, "Microelectronic Circuits", Saunders College Publishing, 1990.

[18] V. Gupta, "Toward the Development of a Non-Invasive Pressure-Flow Sensor System for the Detection of Prostate Cancer in Men", IEEE ISIS at Austin, Oct 9-11, 1996, 81-88.

[19] T. Baumeister, E.A. Avallone, "Mark's standard Handbook for Mechanical Engineers", McGraw-Hill Book Company.